SLAC-PUB-1009
(TH) and (EXP)
January 1972

COMPARISON OF MUON-PROTON AND ELECTRON-PROTON INELASTIC SCATTERING*

T. J. Braunstein,** W. L. Lakin, F. Martin,
M. L. Perl, W. T. Toner,† and T. F. Zipf

Stanford Linear Accelerator Center
Stanford University, Stanford, California 94305

ABSTRACT

Measurements of the differential cross section for the inelastic scattering of 12 GeV/c muons on protons are reported. These measurements cover a kinematic range of $|q^2|$ (the square of the four momentum transferred from the lepton) up to 4.0 $(\text{GeV/c})^2$ and of muon energy losses (ν) up to 9.0 GeV. Only the scattered muon is observed in an optical spark chamber apparatus. The data is compared to electron-proton inelastic scattering, and analyzed in terms of possible lepton form factors and anomalous interactions. μ-p inelastic scattering is found to exhibit the same mild $|q^2|$ behavior as does e-p inelastic scattering. No experimentally significant deviation from the predictions of muon-electron universality has been found. If the ratio of muon to electron inelastic cross sections is parameterized by the form $\left(1.0 + |q^2|/\Lambda_D^2\right)^{-2}$, we find with 97.7% confidence, $\Lambda_D > 4.1$ GeV/c. The muon-proton cross sections on the average are slightly smaller than the electron-proton cross sections. This observation is not experimentally significant because such a difference might be caused by systematic errors; but this observation is used to speculate as to the most fruitful direction for future experiments.

---

*Work supported by the U. S. Atomic Energy Commission.

**An expanded version of this paper was submitted to Stanford University as partial fulfillment of the requirements for Ph.D. degree.

†Present address: Rutherford High Energy Laboratory, Chilton, England.

(Submitted to Phys. Rev.)

I. INTRODUCTION

In this paper we describe an experiment on muon-proton inelastic scattering at 12 GeV/c incident muon momentum.[1] The term muon-proton inelastic scattering describes all those processes in which the incident muon is not absorbed and two or more hadrons are produced. Examples of such processes are

$$\mu+p \rightarrow \mu+n+\pi^+ ,$$

$$\mu+p \rightarrow \mu+\Lambda^o+K^+ ,$$

$$\mu+p \rightarrow \mu+p+\pi^++\pi^- .$$

This paper has two purposes: first to present our measurements of muon-proton inelastic scattering, and second to compare them with similar measurements of electron-proton inelastic scattering. The object of the comparison was to search for hitherto undetected differences between the muon and the electron. Such differences might provide clues to the relationship between these particles. They might also provide information as to whether the muon and the electron are point Dirac particles. And they might lend insight into the fundamental nature of the charged leptons.

We have found no experimentally significant difference between the behavior of the muon and the electron in the inelastic scattering process. Therefore this experiment agrees with other experiments that the muon may be regarded as a point Dirac particle. However, within the overall normalization uncertainty of the comparison the muon-proton inelastic cross sections are on the average lower than the electron-proton inelastic cross sections. The same effect has been found in two measurements of

muon-proton elastic scattering[2,3] when these measurements are compared with electron-proton elastic scattering. The normalization problems in all these comparisons are such that the muon-electron difference might be ascribed to experimental difficulties. Yet, these differences may provide a clue as to most fruitful direction for future experimentation. Therefore in Section VIII we speculate as to the significance of these possible differences in cross sections.

The experiment was carried out at the Stanford Linear Accelerator Center using a momentum analyzed beam of 12 GeV/c positive muons. The apparatus consisted of a liquid hydrogen target, optical spark chambers, scintillation counters and a large analyzing magnet. A full description of the beam[4] and brief description of the apparatus and the results have been published previously.[1,5,6]

Section II contains a summary of what is known about the relative properties of the muon and electron, and thus provides an introduction to what has often been called "the muon-electron puzzle." Those aspects of the theory of charged lepton-proton inelastic scattering which depend only on quantum electrodynamics are given in Section III. In Section IV the experimental apparatus and method are described. The analysis of the muon-proton inelastic data is described in Section V and the results of that analysis are given in Section VI. Section VII consists of a comparison of muon-proton and electron-proton inelastic scattering using a conventional approach. The paper concludes in Section VIII with a more speculative analysis.

II. THE MUON-ELECTRON PUZZLE AND THE PURPOSES OF THE EXPERIMENT[7]

A. Muon-Electron Universality

The muon (μ) and the electron (e), the only known charged leptons, have a wide range of properties in common which are summarized in Table I. Despite this broad similiarity they differ drastically in two respects. First, the muon mass is over 200 times the electron mass. And second, the muon and the electron have internal quantum numbers called lepton numbers[8] which are intrinsically different and are separately conserved in all interactions. The only other particle possessing the muon lepton number is the neutrino (ν_μ) associated with the muon. The electron neutrino (ν_e) is similiarly associated with the electron.

The similiarities and the differences between the muon and the electron are summarized by the principle of muon-electron universality.[7] Except for the difference in mass, and its effects, the muon and the electron have the same properties and behavior in all interactions under the equivalence:

$$\mu^-(\mu^+) \longleftrightarrow e^-(e^+) \tag{1}$$

and

$$\nu_\mu(\bar{\nu}_\mu) \longleftrightarrow \nu_e(\bar{\nu}_e) \quad . \tag{2}$$

We are primarily concerned with the electromagnetic and strong interaction aspects of muon-electron universality. Later in this paper we will discuss some of the evidence for universality from these sources. For a discussion of the role of the weak interaction we refer the reader to the reviews[8,9,10] given in the references.

The generality of the principle of muon-electron universality has led many physicists to speculate as to possible connections between the muon and the electron. One speculation is that they are manifestations of a single particle split into two mass levels by an unknown force. But how then can one explain the very strict lepton number conservation rule which separates electrons from muons? Another speculation is that the electron and the muon are the lowest mass members of a larger family of leptons.

$$e,\ \mu,\ \mu',\ \mu''\ \ \ldots$$

with associated neutrinos

$$\nu_e,\ \nu_\mu,\ \nu_{\mu'},\ \nu_{\mu''}\ \ \ldots\ \ .$$

Of course, there is also the possibility that the muon and the electron have no connection. But then we are faced with the question as to why neutrinos are associated with both of these particles, and no others. We have no evidence as to the validity of any of these speculations. For example, no heavy leptons have been found[7,12,13] and definitive searches using methods such as μ' pair production in electron-positron colliding beams have yet to be done.[14]

B. Point Particles, Form Factors and Strong Interactions

Another aspect of the muon-electron relationship is the belief that the muon and electron are both point Dirac particles. By this we mean that they enter the Dirac equation and all of quantum electrodynamics as mathematical point charges. Some higher order terms in quantum electrodynamics do lead to effects similar to those which might be ascribed to a nonzero size but we do not regard these effects as equivalent to an intrinsic particle size.

The belief in the point nature of the leptons is directly related to the observations that neither the muon nor the electron directly take part in the strong interactions. The hadrons, on the other hand, participate in the strong

interaction and their size is believed to be roughly given by the range of the strong force. Of course, some as yet undiscovered interaction may exist; this interaction being associated with a small but nonzero size for one or both of the charged leptons.

The size and structure of elementary particles cannot be described simply because the description must be both quantum mechanical and relativistic. However, a rough intuitive picture can be developed by considering a nonrelativistic particle with mass or charge density D(r). D(r) is normalized so that

$$\int D(\vec{r})\, d^3r = 1 \,. \tag{3}$$

Next we define the three-dimensional Fourier transform or elastic form factor[15]

$$F(\vec{q}) = \int D(\vec{r})\, e^{-i\vec{q}\cdot\vec{r}}\, d^3r \quad . \tag{4}$$

If the right-hand side of Eq. (4) is expanded in a series we obtain:

$$F(\vec{q}) = 1 - \frac{1}{6}\langle r^2\rangle \cdot |\vec{q}|^2 + \frac{1}{120}\langle r^4\rangle |\vec{q}|^4 - \ldots \quad . \tag{5}$$

Thus $D(\vec{r})$, or $F(\vec{q})$, specifies the nonrelativistic mass or charge density. Again from the nonrelativistic viewpoint, a point particle is specified by $F(\vec{q}) = 1$ or by $D(\vec{r}) = \delta(\vec{r})$, where δ is the Dirac delta function.

The elastic form factor $F(\vec{q})$ also has a direct physical meaning in Coulomb elastic scattering. Consider the elastic scattering of a relativistic Dirac electron on a very heavy, spinless, target particle of mass M and charge e (Fig. 1). The incident (scattered) electron has laboratory three-momentum $\vec{p}$ ($\vec{p}'$) and laboratory energy E (E'). If the target particle is also a point particle the differential cross section in the laboratory system is

given by

$$\left(\frac{d\sigma}{d\Omega}\right)_{NS} = \frac{\alpha^2 \cos^2 \theta/2}{4E^2 \sin^4 \theta/2} \frac{1}{1+(2E/M) \sin^2 \theta/2} \quad . \tag{6}$$

Here θ is the laboratory scattering angle of the electron and α is the fine structure constant. The subscript NS means that the target particle has no spin. (In this paper we use units such that $\hbar = 1$, $c = 1$.) As shown in Fig. 1 the scattering takes place through the exchange of a virtual photon of laboratory three-momentum $\vec{q} = \vec{p} - \vec{p}'$. $\vec{q}$ is the three-momentum transferred from the electron to the target particle. The behavior of the target particle can be treated nonrelativistically if $|\vec{q}|^2 \ll M^2$.

If the target particle is not a point, but has a charge distribution given by D(r), then Eq. (6) becomes[15]

$$\left(\frac{d\sigma}{d\Omega}\right) = \left(\frac{d\sigma}{d\Omega}\right)_{NS} F^2(\vec{q}) \quad , \tag{7}$$

where $F(\vec{q})$ is given by Eq. (4). Thus the elastic form factor directly gives the effect of the particle's charge distribution on the elastic differential cross section. In going to a fully relativistic description we must replace $F(\vec{q})$ by a function of a Lorentz kinematic invariant. That invariant is q^2, the square of the four-momentum transferred from the lepton and carried by the proton. In our metric q^2 is given by

$$q^2 = (E-E')^2 - (\vec{p}-\vec{p}')^2 \quad . \tag{8}$$

By conservation of energy and momentum

$$q^2 = -2M(E-E') \quad ,$$

so that

$$q^2 \leq 0 \quad .$$

We refer to this negative q^2 as spacelike. The relativistic analogue of Eq. (7) is then

$$\left(\frac{d\sigma}{d\Omega}\right) = \left(\frac{d\sigma}{d\Omega}\right)_{NS} G^2(q^2) \tag{9}$$

where $G(q^2)$ is the relativistic analogue of $F(\vec{q})$. Furthermore we say that relativistically we have a point particle if

$$G(q^2) = \text{Constant} \quad . \tag{10}$$

We can also expand

$$G(q^2) = a_0 + a_1 |q^2| + a_2 |q^2|^2 + \quad \ldots \tag{11}$$

in analogy to Eq. (5). But unless $|q^2|$ is small compared to M^2, there is no nonrelativistic interpretation of the coefficients analogous to the interpretation of Eq. (5).

The most common extension of Eq. (9) is electron-proton elastic scattering where the differential cross section is given by the Rosenbluth formula[15,16]

$$\left(\frac{d\sigma}{d\Omega}\right)_{ep,\,elastic} = \left(\frac{d\sigma}{d\Omega}\right)_{NS} \left[\frac{G_E^2(q^2) + \tau\, G_M^2(q^2)}{1+\tau} + 2\tau\, G_M^2(q^2) \tan^2 \theta/2\right] \quad , \tag{12}$$

for a point electron $(d\sigma/d\Omega)_{NS}$ is defined in Eq. (6) and $\tau = |q^2|/4M^2$. The anomalous magnetic structure[15] of the proton leads to two elastic form factors, $G_E(q^2)$ and $G_M(q^2)$, for the proton. Experimentally it is found[16] that

$$G_E(q^2) \approx 1/\left[1 + |q^2|/.71\right]^2 \tag{13}$$

and

$$G_M(q^2) \approx 2.79\, G_E(q^2) \quad .$$

(In this article energy units will always be GeV, momentum units will be GeV/c and the units of q^2 will be $(\text{GeV/c})^2$.) Continuing the example, for very small values of $|q^2|$

$$G_E(q^2) \approx 1 - |q^2|/.355 \quad .$$

Comparing with the nonrelativistic expression, Eq. (5),

$$\langle r^2 \rangle^{1/2} \approx .8 \times 10^{-13} \text{ cm} \tag{14}$$

is the root mean square radius of the proton.

If the charged lepton, ℓ, is not a point particle, then like the proton, there may be two elastic form factors associated with it,[17] But in our present state of ignorance it is sufficient to assign to the charged lepton the single elastic form factor $G_\ell(q^2)$. Then Eq. (9) would become

$$\left(\frac{d\sigma}{d\Omega}\right) = \left(\frac{d\sigma}{d\Omega}\right)_{NS} G^2(q^2)\, G_\ell^2(q^2) \quad .$$

And the Rosenbluth formulas would also be modified by a multiplicative factor $G_\ell^2(q^2)$ on the right-hand side of Eq. (12).

It has become conventional[18,19,20] to take a form for $G_\ell(q^2)$ analogous to the proton form factor and write

$$G_\ell(q^2) = 1/\left[1 - q^2/\Lambda_\ell^2\right] \quad , \tag{15a}$$

$$G_\ell(q^2) = 1/\left[1 + |q^2|/\Lambda_\ell^2\right] \quad , \qquad \text{for } q^2 \text{ spacelike} \; . \tag{15b}$$

Note however that unlike Eq. (13), only the first power of $\left[1 + |q^2|/\Lambda_\ell^2\right]$ appears in the denominator. Equation (15a) has some theoretical significance in that it has the same form as the denominator of the propagator of a particle of mass Λ_ℓ. Equation (15a) also offers some theoretical convenience in that it is similiar to the regulated propagator used to cure divergences in quantum electrodynamics.[18,20] Λ_ℓ is an inverse measure of the deviation of the muon from a point particle. For very small $|q^2|$, namely $|q^2| \ll m_\ell^2$, Eq. (5) yields

the nonrelativistic interpretation

$$\langle r^2 \rangle_\ell^{1/2} = \sqrt{6}/\Lambda_\ell \quad . \tag{16}$$

Of course, if the lepton ℓ is a point Dirac particle, $G_\ell(q^2) = 1$ for all values of q^2. We have emphasized that Eq. (15) gives the conventional function for $G_\ell(q^2)$, other functions are discussed in Section VIII.

Returning to the question of muon-electron universality, it is clear that the principle is preserved if

$$G_\mu(q^2) \equiv G_e(q^2) \quad . \tag{17}$$

But if $G_\mu(q^2) \neq G_e(q^2)$ then (1) muon-electron universality is violated and (2) either the muon or the electron or both are not point particles.

C. Special Interactions of the Muon or the Electron

The principle of muon-electron universality may also be violated if only the electron or only the muon has a special interaction other than the weak or electromagnetic. Such speculations generally take the form of an assumption,[21,22] that the muon has an anomalous interaction with a neutral particle. This anomalous interaction is then the cause of the difference between the masses of the muon and the electron. This type of speculation is discussed further in Section VIII. We wish to make only two comments here. First, it is equally reasonable to speculate that the anomalous interaction is associated with the electron, or is associated with both particles through different coupling constants. Second, if the form factor $G_\ell(q^2)$ is found to be different from one for some values of q^2, this may be interpreted as an indication that the lepton ℓ has some anomalous interaction.

D. Some Tests of the Principle of Muon-Electron Universality

1. Electric Charge

Using measurements[10] of the muon magnetic moment, the muon gyromagnetic ratio (g_μ), muon X-ray spectra and the electron's charge; the ratio of muon's electric charge (e_μ) to the electron's electric charge (e_e) is calculated to be[10] $e_\mu/e_e = 1 \pm (4 \times 10^{-5})$.

A much lower limit can be obtained[23] by observing that if charge is conserved in the muon decay process $\mu \rightarrow e + \nu_\mu + \bar{\nu}_e$ then one or both neutrinos will have a nonzero charge if $e_\mu \neq e_e$. Astrophysical considerations then set an upper limit on the charge that can be possessed by a neutrino. This leads to the limit $e_\mu/e_e = 1 \pm (1 \times 10^{-13})$.

2. Gyromagnetic Ratio

The gyromagnetic ratio, g_ℓ, can be calculated exactly from quantum electrodynamics, once the lepton mass is known, if the very small contributions from electromagnetic coupling to strongly interacting particles are ignored. It is conventional to set

$$(g_\ell - 2)/2 = a_\ell \quad .$$

The most recent measurements of E. Picasso[24] and his colleagues on g_μ yield

$$a_\mu^{exp} = (116616 \pm 31) \times 10^{-8} \quad ,$$

and quantum electrodynamics yields[11]

$$a_\mu^{theory} = (116587 \pm 3) \times 10^{-8} \quad .$$

Thus experiment and theory for the muon are in agreement. Even more precise agreement is found for the electron.[25]

To summarize, the static properties of the muon (only some of which have been discussed here) compared to the static properties of the electron

show no differences other than those explained by the mass difference. Furthermore, the static properties are those of point Dirac particles.

3. Charged Lepton-Proton Elastic Scattering

Although the static properties of the charged leptons show no unexplained differences, one might hope[7] that differences will appear when the dynamic properties of the charged leptons are measured in high energy reactions. One such reaction, which is closely connected with our experiment, is the elastic scattering of a charged lepton ℓ on a proton.

Numerous electron-proton elastic scattering experiments[16] and two muon-proton elastic scattering experiments[2,3] have been performed. Comparison of these experiments do not show any definitely significant deviations from muon-electron universality. This conclusion is discussed in detail in Section VII.

4. Other High Energy Tests

A large number of tests of quantum electrodynamics have been carried out which either do not involve hadrons at all or only involve hadrons as sources of a low $|q^2|$ virtual photon. Examples of such tests are the colliding beam reactions

$$e^- + e^- \rightarrow e^- + e^- ,$$
$$e^- + e^+ \rightarrow e^- + e^+ ,$$
$$e^- + e^+ \rightarrow \mu^- + \mu^+ ;$$

we will use the results of some of those colliding beam experiments in Section III.B. Other examples are the Bethe-Heitler pair production process

$$\gamma + \text{Nucleus} \rightarrow \text{Nucleus} + \ell^+ + \ell^- ,$$

and the bremsstrahlung process

$$\ell + \text{Nucleus} \rightarrow \ell + \gamma + \text{Nucleus}.$$

Two excellent reviews[11] of these processes have appeared recently. We only remark here that no deviations were found from quantum electrodynamics or from the point particle nature of the leptons. Therefore these experiments confirm the principle of muon-electron universality.

E. Purposes of the Experiment

In the foregoing discussion of the muon-electron puzzle we have implicitly given the purposes of our experiment. Therefore we only summarize them here. The purposes of the experiment are, by comparison of muon-proton and electron-proton inelastic scattering to

1. search for hitherto unknown differences between the muon and the electron,
2. test the principle of muon-electron universality,
3. test the point particle nature of the muon compared to that of the electron, and
4. search for anomalous interactions of the muon.

As we have emphasized these searches and tests are related.

In performing this experiment we have extended the search for a violation of muon-electron universality to a new region of the kinematic plane. In elastic scattering $\nu = |q^2|/2M$ (where ν is the energy loss of the lepton in the laboratory frame), but in inelastic scattering $\nu > |q^2|/2M$. Thus ν and q^2 may be varied independently, allowing the exploration of a much larger kinematic region. Further, by measuring only the inelastically scattered lepton we place no restrictions on the nature of the final hadronic state. It is conceivable that a violation of muon-electron universality which involves hadrons would be more easily seen in inelastic scattering than in elastic scattering. Finally, one of the more unexpected results of μ-p and e-p inelastic scattering

was the large cross section, compared to elastic scattering, at high $|q^2|$. Because of this larger q^2 range, inelastic scattering provides a greater sensitivity to lepton form factors or to those anomalous interactions which would modify the q^2 behavior of one lepton cross section relative to the other.

III. THEORY OF THE EXPERIMENT

A. Basic Concept and Kinematics

Consider the reaction shown schematically in Fig. 2 in which two or more hadrons are produced by the inelastic scattering of an unpolarized muon on an unpolarized target proton. A general inelastic experiment would consist of the detection and study of the various hadronic states which are produced. We have, however, carried out a much more restricted inelastic experiment in which we only detect the scattered muon. Explicitly, let the laboratory three-momentum and laboratory energy of the incident muon be $\vec{p}$ and E respectively. Let the equivalent properties of the scattered muon be $\vec{p}'$ and E'. The experiment consists of:

1. fixing $\vec{p}$,
2. detecting only the scattered muon ,
3. not detecting any of the hadrons produced, and
4. measuring $\vec{p}'$.

The experiment then measures the distribution of $\vec{p}'$ as a function of $\vec{p}$ and $\vec{p}'$.

The absence of polarization means that the distribution of $\vec{p}'$ is cylindrically symmetric about $\vec{p}$. This observation plus the isotropy of space means that the scattering is completely described by just three kinematic quantities. One convenient choice for these quantities is

p = absolute magnitude of $\vec{p}$,

$\nu = E - E'$

and

$$q^2 = (E - E')^2 - (\vec{p} - \vec{p}')^2$$

ν is the energy lost by the lepton in the laboratory system. q^2, the square of the four-momentum transferred from the lepton to the hadronic system, has been discussed in Section II. As in elastic scattering, q^2 is negative in our metric. Using these variables the distribution of $\vec{p}$ is described by the double differential cross section $d^2\sigma/dq^2 d\nu$, a function of p, q^2 and ν.

The total invariant mass of the produced hadrons, called M*, is given by

$$M^{*2} = (E + M - E')^2 - (\vec{p} - \vec{p}')^2$$

where M is the proton mass. This reduces to

$$M^{*2} = M^2 + 2M\nu - |q^2| \tag{18}$$

so that ν and q^2 fix M*. We note that $M^{*2} > M^2$ for inelastic scattering. Therefore

$$|q^2| < 2M\nu \quad . \tag{19}$$

Returning to Fig. 2 we see that in measuring only the outgoing muon the experiment automatically sums over all hadronic states whose total invariant mass M* is given by Eq. (18).

The principle of muon-electron universality can then be tested by comparing $d^2\sigma_\mu/dq^2 d\nu$ for the muon-proton system with $d^2\sigma_e/dq^2 d\nu$ for the electron-proton system. If the muon and the electron had the <u>same</u> mass, the principle would predict

$$\frac{d^2\sigma_\mu}{dq^2 d\nu}(p, q^2, \nu) = \frac{d^2\sigma_e}{dq^2 d\nu}(p, q^2, \nu) \quad . \tag{20}$$

Testing this equality for various values of p, q^2, and ν tests the validity of the principle. This then is the basic concept of the experiment and of the comparison.

Two factors prevent the direct use of Eq. (20). First, the muon and electron have different masses. This difference, though it has only a small effect on the cross sections, must be accounted for in the comparison. Second, the sets of values of p, q^2 and ν which occurred in our experiment were not identical to the sets of values of p, q^2 and ν which occurred in the electron-proton experiment used for the comparison. Therefore it is necessary to interpolate $d^2\sigma_e/dq^2d\nu$. These two objectives can be achieved through the use of the one photon exchange explanation of charged lepton-proton inelastic scattering. There is an additional benefit from the use of the one photon exchange explanation. We will find that this explanation will enable us to have a more physical understanding of the significance of the comparison.

B. One Photon Exchange

The inelastic scattering of charged leptons on protons leading to the production of hadrons takes place almost entirely through the exchange of a single virtual photon as shown in Fig. 2. The contribution of two photon exchange, Fig. 3, to the inelastic cross section is believed to be at most a few percent for three reasons. First, the two photon diagram has an additional factor of $\alpha/\pi \approx 1/500$ compared to the one photon diagram. It is not at present possible to accurately calculate the magnitude of the two hadronic vertices in Fig. 3 compared to the single hadronic vertex in Fig. 2. But it is believed that this cannot compensate for the additional α/π factor. Second, the contribution of the two photon diagram to elastic scattering has never been experimentally detected and is less than 2%.[16] And, third, some indication that two photon exchange in inelastic scattering is at most a few percent effect (but not necessarily undetectable) has been given by an experiment[26] searching for T-violation in inelastic electron scattering.

Therefore we return our attention to the one photon exchange diagram, Fig. 2. For this diagram Lorentz and gauge invariance considerations[27,28] lead to the conclusion that the differential cross section $d^2\sigma/dq^2d\nu$ depends on explicit factors involving all the kinematic variables and just two independent quantities which must be experimentally determined. These quantities, functions of only q^2 and ν, describe in a summary way the production of hadrons in the interaction of virtual photons with protons. The separation of the kinematic factors is to some extent arbitrary. In this paper we use primarily the definition and separation introduced by Hand.[29]

Hand first defines the kinematic quantity

$$K = \nu - |q^2|/2M \quad , \tag{21}$$

where M is the proton mass. Then Eq. (18) can be rewritten as

$$M^{*2} = M^2 + 2MK \ .$$

Thus K is the energy that a real photon must have to give the same total energy, M*, in the photon-proton center-of-mass system. We note that any function of q^2 and ν can be written as a function of q^2 and K, and that $K > 0$. Hand then defines the two independent quantities $\sigma_T(q^2,K)$ and $\sigma_S(q^2,K)$ through the equations

$$d^2\sigma_\ell/dq^2d\nu = d^2\sigma_\ell/dq^2dK = \Gamma_T(q^2,K,p,m_\ell)\,\sigma_T(q^2,K) + \Gamma_S(q^2,K,p,m_\ell)\,\sigma_S(q^2,K) \quad , \tag{22}$$

$$\Gamma_T = \left(\frac{\alpha}{2\pi|q^2|}\right)\left(\frac{K}{p^2}\right)\left(1 - \frac{2m_\ell^2}{|q^2|} + \frac{2EE' - |q^2|/2}{(E-E')^2 + |q^2|}\right) \tag{23}$$

and

$$\Gamma_S = \left(\frac{\alpha}{2\pi|q^2|}\right)\left(\frac{K}{p^2}\right)\left(\frac{2EE' - |q^2|/2}{(E-E')^2 + |q^2|}\right) \quad . \tag{24}$$

Here $p = |\vec{p}|$ and m_ℓ is mass of the lepton ℓ. Γ_T and Γ_S are the virtual photon fluxes for transverse and scalar photons, respectively. Thus $\sigma_T(q^2, K)$ and $\sigma_S(q^2, K)$ which may be thought of as the total cross sections for the interaction of transverse and scalar photons respectively with protons. These σ's have the properties[29] that as q^2 goes to zero, $\sigma_S(q^2, K)$ goes to zero and $\sigma_T(q^2, K)$ goes to $\sigma_{\gamma p}(k)$ — the total cross section for the interaction of a physical photon of energy K with a proton. Next we define ϵ, the ratio of the virtual photon fluxes, by

$$\epsilon(q^2, K, p, m_\ell) = \Gamma_S/\Gamma_T = \left(\frac{2EE' - |q^2|/2}{(E-E')^2 + |q^2|}\right) \Big/ \left(1 - \frac{2m_\ell^2}{|q^2|} + \frac{2EE' - |q^2|/2}{(E-E')^2 + |q^2|}\right) . \tag{25}$$

Then

$$d^2\sigma_\ell/dq^2 dK = \Gamma_T(q^2, K, p, m_\ell)\left[\sigma_T(q^2, K) + \epsilon(q^2, K, p, m_\ell)\,\sigma_S(q^2, K)\right] \quad . \tag{26}$$

In our experiment we cannot, using only our own data, separate σ_T from σ_S. Therefore we shall report and use for the comparison

$$\sigma_{exp,\ell}(q^2, K, p) = \sigma_T(q^2, K) + \epsilon(q^2, K, p, m_\ell)\,\sigma_S(q^2, K) \quad . \tag{27}$$

We note that

$$\sigma_{exp,\ell}(q^2, K, p) = \left[d^2\sigma_\ell/dq^2, dK\right]/\Gamma_T(q^2, K, p, m_\ell) \quad . \tag{28}$$

As mentioned before, the separation of empircal functions from the kinematics is to some degree arbitrary. Another form which is in current use is

that defined by Von Gehlen[27] and Drell and Walecka.[28] Here

$$\frac{d^2\sigma_\ell}{dq^2 dK} = \frac{2\pi\alpha^2}{q^4}\,\frac{|\vec{p}'|}{E'|\vec{p}|^2}\left[2\left(EE' - |\vec{p}|\,|\vec{p}'|\cos\theta - 2m_\ell^2\right) W_1(q^2,K)\right.$$

$$\left. + \left(EE' + |\vec{p}|\,|\vec{p}'|\cos\theta + m_\ell^2\right) W_2(q^2,K)\right] \quad . \tag{29}$$

$W_1(q^2,K)$ and $W_2(q^2,K)$, which are the analogues of the proton elastic form factors, are related to the total cross sections by the equations:

$$W_2(q^2,K) = \frac{1}{4\pi^2\alpha}\left[\frac{K|q^2|}{\nu^2+|q^2|}\right]\left[\sigma_T(q^2,K) + \sigma_S(q^2,K)\right], \tag{30}$$

$$W_1(q^2,K) = \frac{1}{4\pi^2\alpha}\,K\sigma_T(q^2,K) \quad .$$

In Section VI we give our results in terms of $W_1(q^2,K)$ and $W_2(q^2,K)$, as well as in terms of $\sigma_T(q^2,K)$ and $\sigma_S(q^2,K)$.

All of the above is based on the assumption that the lepton is a point Dirac particle. If that is not the case, the cross section equations must be modified. In particular, Eq. (26) would change, at least to the form

$$d^2\sigma_\ell/dq^2 dK = \Gamma_T(q^2,K,p,m_\ell)\left[\sigma_T(q^2,K) + \epsilon(q^2,K,p,m_\ell)\,\sigma_S(q^2,K)\right] G_\ell'^2(q^2,K) \quad . \tag{31}$$

Here $G_\ell'(q^2,K)$ like the other inelastic structure functions can be a function of both q^2 and K. $G_\ell'(q^2,K)$ is an extension of $G_\ell(q^2)$ the elastic form factor but there is no relation required between $G_\ell'(q^2,K)$ and $G_\ell(q^2)$. The statement $G_\ell'(q^2,K) \equiv G_\ell(q^2)$ has no direct physical meaning. Equation (27) now becomes

$$\sigma_{exp,\ell}(q^2,K,p) = \left[\sigma_T(q^2,K) + \epsilon(q^2,K,m_\ell)\,\sigma_S(q^2,K)\right] G_\ell'^2(q^2,K) \quad . \tag{32}$$

To test muon-electron universality we define the ratio

$$\rho_{\text{inelastic}}(q^2, K, p) = \sigma_{\text{exp},\mu}(q^2, K, p)/\sigma_{\text{exp},e}(q^2, K, p)$$

$$= \frac{\left[\sigma_T(q^2, K) + \epsilon(q^2, K, p, m_\mu)\sigma_S(q^2, K)\right] G'^2_\mu(q^2, K)}{\left[\sigma_T(q^2, K) + \epsilon(q^2, K, p, m_e)\sigma_S(q^2, K)\right] G'^2_e(q^2, K)} . \tag{33}$$

To relate $\rho_{\text{inelastic}}$ to the ratio $G'^2_\mu(q^2, K)/G'^2_e(q^2, K)$ it is obviously necessary to cancel out the terms in the square brackets in Eq. (33). How we do this is discussed in detail in Section VII.

IV. THE EXPERIMENTAL METHOD

A. General Description

The differential cross section, $d^2\sigma_\mu/dq^2dK$, for the inelastic scattering of muons by protons is a function of three independent kinematic variables. The set that is directly accessible to the experimentalist consists of the incident and final muon momenta and the muon angle of scatter. In this experiment the momentum of the incident muon was fixed at 12 GeV/c. The final muon was detected if its momentum was in the range of 3 to 12 GeV/c and if its scattering angle was in the range of 30 to 240 mrad. At the beginning of the experiment some data was taken at 10 GeV/c incident momentum.[6] This 10 GeV/c data will be used in this paper for the study of systematic errors.

The muon beam was photoproduced in a water-cooled copper target by bremsstrahlung from 16 GeV/c electrons. In muon-proton inelastic scattering experiments the pion contamination in the muon beam must be very small because the cross section for pions interacting with protons to produce hadrons is 10^4 times the same cross section for muons interacting with protons. In this experiment the pion contamination was made very small by passing the beam through 5.5 m of berylium which followed the copper target. This beryllium "pion filter" reduced the pion contamination from 30% in the production target to 3×10^{-6} pions per muon in the final beam. An additional factor of 50 in pion rejection was achieved in the apparatus itself, as described later. The beam magnets momentum analyzed and focused the muons yielding a momentum resolution of $\pm 1.5\%$ and a phase space of 5×10^{-3} cm^2 sr. Although the beam was capable of higher intensity, for most of the experiment 160 muons per 1.4 μsec accelerator pulse was used. Usually 180 pulses per

sec were delivered to the experiment giving an average intensity of 30,000 muons per sec.

The apparatus is illustrated in Fig. 4. The liquid hydrogen target was a mylar cylinder 198 cm long and 18 cm in diameter. Immediately above and behind the target was a 1.2 kG-meter magnet whose function was to sweep electrons from μ-e elastic scatters in the hydrogen away from the first two spark chambers.[30] The sweep magnet was unfortunately not completely equal to the job as the spray of electron tracks in chambers 1 and 2 imposed an upper limit on the beam intensity. This upper limit was in the range of 60,000 muons per sec. The scattered muon was detected and its vector momentum measured by a muon spectrometer consisting of eight large optical spark chambers, three planes of trigger scintillation counters and a large momentum analyzing magnet. Chambers 1 and 2 determined the angle of the scattered muon relative to the incident beam line. Chambers 1, 2, 3, and 4 measured the deflection of the muon as it passed through the magnet, and hence the outgoing muon momentum. The spark chambers were triggered and photographed whenever there was a coincidence between selected pairs of counters in the first two trigger planes and any counter in the third plane. There were also some veto counters which will be described later.

The additional factor of 50, by which pions were rejected in the apparatus, was obtained in the following way. Chambers 4 and 5 were separated by a total thickness of 61 cm of steel. In addition, chambers 6 through 8 were each preceded by a steel slab 16.5 cm thick. Thus for hadronic particles there were eleven geometric collision lengths between chambers 4 and 8. Therefore pions or other hadrons would be absorbed before reaching chamber 8. On the other hand since the probability of high energy muons interacting in the steel

was very small, the muons reached chamber 8 having only undergone multiple scattering. A pion could only cheat the system by decaying to a muon before it reached chamber 4. The average probability for such a decay was 2%, hence the rejection factor of 50.

Directly beneath the hydrogen target was another thin plate spark chamber. Its function was to record the angle of the recoil proton from elastic mu-p scatters. This gave us the capacity to concurrently measure the elastic as well as the inelastic cross sections. We have not yet completed the calculation of the elastic cross section. We have however used the large sample of elastic events to study the resolution and the systematics of the experiment, and to provide a direct measure of the beam momentum.

The measurement of the cross section required an absolute count of the number of incident particles. The instantaneous muon beam rate was too high to permit the counting of individual muons. Instead we used a high current beam monitor, which consisted of five small scintillation counter telescopes. This device detected approximately one in thirty beam muons. The precise fraction sampled was determined on a roll by roll basis by performing calibration runs roughly six times a day. During the calibration the beam intensity was one to two muons per pulse so that two conventional whole beam telescopes could be compared to the high current monitor.

Rolls of data were run with the target empty a number of times each day as part of the regular running sequence in order to continuously monitor background events not originating in the hydrogen of the target.

The 12 GeV/c data results from 2.4×10^{10} muons incident on the full hydrogen target and $.5 \times 10^{10}$ muons on the empty target. Corresponding

numbers for the 10 GeV/c data are 7.9×10^8 and 6.1×10^8. In all some 346,000 photographs were taken for the data sample.

B. The Beam

The muon beam is described in detail in Ref. 4. The dominant process by which the muons were produced consisted of two steps, both occurring in the same target. First a photon was produced by the bremsstrahlung of a 16 GeV electron in the field of a nucleus. Then the photon, in the field of a second nucleus, produced a pair of muons. The direct production of muon pairs by electrons was negligible in comparison to this two-step process. In marked contrast to muon beams produced by pion decay at proton accelerators, the source of muons in this experiment had a small cross-sectional area equal to that of the incident electron beam, namely, 5 mm by 5 mm. It was therefore possible to make a muon beam with optical properties similar to those of high energy hadron beams.

The choice of the target material, copper, was dictated by the desire to produce the most favorable ratio of muons to pions. This is discussed in Ref. 4. The bulk of the muon production occurred, and 70% of the power in the electron beam was dissipated in the first 4 radiation lengths of the 11.6 radiation length, water cooled target. The remaining 30% of the power was in electron-photon showers which left the target in the forward direction. These showers were sufficiently degraded in energy by this point that there was negligible particle production in the beryllium "pion filter" that immediately followed the copper target. The beryllium filter material was chosen to maximize the absorption of hadrons and to minimize the electromagnetic multiple scattering which would increase the phase space of the muon beam.

The pion attenuation in the "pion filter" was measured in a subsidiary experiment. By varying the length of the beryllium filter the attenuation length was measured to be $.47 \begin{smallmatrix}+.03\\-.02\end{smallmatrix}$ meters. This number was found to be independent of momentum above 4 GeV/c. The length of filter used for the μ-p experiment was 5.5 meters, which gave a π/μ ratio $3.0 \begin{smallmatrix}+1.3\\-0.9\end{smallmatrix} \times 10^{-6}$ by extrapolation.

The layout of the beam and the experimental apparatus is shown in Fig. 5. The muon beam was at 0^{o} to the electron beam and had two stages of momentum analysis and three focusing stages. It used six standard BNL 18D72 bending magnets and ten 8Q48 quadrupole focusing magnets arranged in doublets. The momentum resolution, $\Delta p/p = \pm 1.5\%$ was determined by the width of the collimating slit S1 at the first focus. The vertical dimension of the beam was also regulated by S1. The beam, so defined, was kept well clear of the apertures of all subsequent magnets and collimators so as to preserve the phase space against multiple scattering and protect the trigger system from beam spray. The beam was brought to a final focus at the hydrogen target.

Accompanying the muons in the main beam was a lower density "halo" of off-axis and off-angle muons. This halo occurs in all types of beam, but can be particularly troublesome in a muon experiment for two reasons. First, it is difficult to remove the halo muons because they cannot be absorbed by strong interaction processes. Second, those halo muons which reach the apparatus may produce false triggers in an experiment, such as this one, where only one scattered muon is required for a trigger. The low density halo was trimmed and mostly removed at the second focus by a second collimating slit S2. The slits S1 and S2 were made of one meter long steel blocks

arranged to form closed iron circuits around the beam. The steel of slit S2 was magnetized to an internal field of 15 kG in order to sweep off-axis particles further away from the beam channel. The basic optical parameters of the beam are shown in Table II. The effects of chromatic aberrations are negligible. Figures 6 and 7 show the vertical and horizontal beam profiles at the hydrogen target. The tail visible in the left-hand corner of the vertical distribution is an indication of the beam halo mentioned earlier. About 1% of the beam is in a ring between 6 and 9 cm from the center line. Another 1% lay beyond this out to a radius of about 75 cm. Substantial improvements were made in the veto and accidental rates resulting from these halo muons by the liberal use of steel shielding around the final beam stage.

At the conclusion of the experiment small spark chambers were set up directly in the beam and photographs were taken with a low beam intensity. The spatial distributions agreed with Figs. 6 and 7 and the angular distributions are shown in Figs. 8 and 9. These distributions represent the dominant uncertainty in the determination of the scattering angle, approximately ± 4.5 mrad.

C. Scintillation Counter Systems

1. The Trigger System

The trigger system is shown in Fig. 10. Planes A and B were located upstream of the large magnet just in front of chambers 1 and 2, respectively. The four lower counters in each were semicircular annular rings, the two upper counters were rectangular. This arrangement allowed a crude angular selection to be made.

The C plane consisted of fourteen rectangular scintillators 96.5 cm long by 16.5 cm wide by 1.0 cm thick. These were stacked vertically starting

40 cm above the beam line, just upstream of chamber 5 and behind the 61 cm of steel shielding. This arrangement permitted a crude outgoing momentum selection.

The trigger circuitry was arranged so that A, B counter combinations inconsistent with muons scattered from the target were excluded. A trigger $ABC\bar{V}$ consisted of an acceptable A, B coincidence in time with a pulse from any C counter and not in time with any veto pulse, $\bar{V}$. The veto system is described later. This $ABC\bar{V}$ circuit was scaled, as was a parallel, redundant, $ABC\bar{V}$ circuit. We also used an $ABC\bar{V}_{delayed}$ circuit to keep track of random vetoes and an $ABC_{delayed}\bar{V}$ circuit to keep track of accidentals. The trigger pulse set off the spark chambers, flashed the fiducial lamps and data box, and after a suitable delay advanced the camera.

Data was taken with three trigger configurations. One configuration with all counters on was called A2 B2 C1. This trigger configuration was sensitive down to a minimum scattering angle of 30 mrad. Another configuration, called A2 B2 C2, had the bottom C counter turned off. It also was sensitive to a minimum of 30 mrad, but had a lower acceptance for low q^2 elastic scatters. The third configuration, called A3 B3 C2, had the bottom A, B and C counters turned off. This led to a minimum scattering angle of 45 mrad.

The trigger rates were dependent upon the particular trigger condition but a typical rate was one ABC per 1500 beam muons. With the vetoes in anticoincidence it dropped to one $ABC\bar{V}$ per 150,000 beam muons, about 30% being accidentals. Four hundred to 1200 pictures per hour were taken.

2. The Veto System

The function of the veto system was to prevent muons in the beam halo from triggering the spark chambers. Twelve scintillation counters were

placed around the beam at the points (Fig. 5) most likely to intercept such beam halo muons. The veto outputs, called $\bar{V}$, were added, stretched to 50 nsec and put in anticoincidence with both the trigger and normalization systems. The vetoes resulted in a 15% electronic off time.

3. The Normalization System

Low current. Two redundant beam telescopes were used to make an absolute count of beam particles at sufficiently low currents. Each telescope consisted of two scintillation counters (D1 and E3, and D2 and E4) each bigger than the beam.

Each telescope had parallel, redundant logic circuits with dead times made intentionally greater than the intrinsic dead times. These dead times were made different from each other as a consistency check. All of these circuits were scaled. In addition, all were scaled in anticoincidence with the veto system. The dead time correction required was 2-1/2% for each count/pulse or typically 3-1/2%.

High current. The high current monitor was composed of two identical units, each containing five small cylindrical pieces of scintillator connected by air light pipes to 56 AVP phototubes. The scintillators were arranged on the four corners of a square and one in the center. The square was 5 cm on a side, the four outer scintillators were 1 cm in diameter, and 5 mm high. The center one was .707 cm in diameter and 5 mm high.

The two units were attached (the two scintillator planes separated by 15 cm) and mounted on a stand in the beam 4.7 m upstream of the third focus. Corresponding phototubes were put in electronic coincidence to form five counter telescopes which were all scaled. (The center telescope was scaled through a second complete circuit with a longer dead time as a check.) In

addition, the sum of the telescopes was also scaled (again duplicate circuits with different dead times).

The center telescope sampled the high current center of the beam while the other four sampled the lower current edges. (The beam was less sharply defined at the location of the beam monitor than it was at the third focus.) A typical rate for the sum of the telescopes was 4/pulse. Typically 42% of the counts came from the center telescope and the rest was divided among the other four, ranging from 25% to 6%. These individual sum ratios proved to be a useful monitor of the beam position and size.

Our normalization procedure consisted of determining the ratio of beam monitor to D2E4$\bar{V}$ counts at low beam current and then assuming that this ratio held true at higher current. This last crucial assumption was tested in a variety of ways. Beam blowup was imitated by changing the settings of the last quadrupole pair and also by turning off the magnetic field in S2. Beam position was shifted by moving the primary electron beam spot around on the target. The conclusion reached from these investigations was that changes in the beam large enough to produce 2% changes in the ratio of the beam monitor to D2E4$\bar{V}$ also produced clear changes in the ratios of the individual telescopes. Further, comparisons of low to high current beams showed no indication of such ratio changes.

At low current, dead time corrections to the beam monitor were negligible, at high current they came to about 3%.

4. General

Commercial electronics modules were used generally in the experiment. All the critical scalers were designed for 100 Mc operation. The entire

electronic system was gated to the beam pulse and everything was shut off during the one third second it took to fire the spark chambers and advance the camera.

D. The Muon Spectrometer

The muon spectrometer consisted of eight spark chambers and a large, momentum analyzing, magnet. The positions of the spark chambers along the beam line, their dimensions and other relevant information are given in Table III.

The first three chambers had "thin plates" made with sheets of 1 mil aluminum foil stretched across aluminum frames. Chambers 1 and 2 had semicircular cutouts at the bottom of the plates to allow passage for the beam. Chambers 4 through 8 had 1.3 cm thick, solid aluminum, plates that served as part of the pion discrimination system. A gas mixture of 90% helium and 10% neon was used. Each chamber was fired by a spark gap that in turn was triggered by a master spark gap. There were two such master gaps, one for chambers 3 through 8 and one for chambers 1 and 2 and the recoil chamber. These chamber groups also had separate high voltage supplies, both of which ran at approximately 15 kV.

The spectrometer was viewed directly by a 70 mm camera located 23.5 m away. The chambers were slightly rotated about a vertical axis to afford a direct view into the gaps to the camera. A 90^{o} stereoscopic view was provided for each chamber by a front silvered mirror mounted beneath it at an approximately 45^{o} angle. These mirrors were autocollimated into alignment. During each photographic exposure the data box and ten principal fiducials were flashed. At the beginning of each role the full set of 63 fiducials, including 53 viewed through the various mirrors, were photographed.

The large analyzing magnet had a 91.4 cm gap and a 137 cm diameter pole face. It was run at a current of 9820 amps which gave a central field of 15,000 gauss and $\int$Bdl of approximately 27 kG meters. The magnet's field was carefully measured at some 21,420 points by the SLAC Magnetic Measurement Group. In addition to a continuous magnet current display the field was regularly checked with a permanently mounted flip coil.

E. Recoil Chamber

The recoil chamber had 67 plates tilted at an angle of 60^{o} to the vertical. The plates were constructed by epoxying two layers of 1 mil aluminum foil to both sides of a sheet of .95 cm close-cell styrofoam. This sheet previously had been epoxyed into an aluminum frame. Electrically the recoil chamber was actually four separate spark chambers, each with its own spark gap. The recoil chamber and its stereo view mirror were viewed by a system of three additional mirrors. Prisms were used to give a view into the gaps in both the direct and stereo views. The image was projected onto the center of the film in the spot occupied by the large magnet.

V. ANALYSIS OF DATA

The data was divided into seven blocks of consecutive rolls on the basis of beam energy, trigger condition and beam current. These blocks were processed as units through the entire analysis. Cross sections were computed separately for each block by an individual SUMX subroutine incorporating its particular corrections. These cross sections were then put through a radiative correction program and only finally were the different blocks merged. The method was both necessary, in that it allowed us to keep track of a great deal of data, and useful because it made possible comparisons of data run and processed at different times under different conditions.

A. Scanning

Scanning and event identification were greatly facilitated by the simplicity of the pictures. During the inelastic phase of the experiment the scanners were instructed to ignore the recoil chamber and to record as an event any frame in which the three principle fiducials and the data box were visible, and a "good muon" was present. A "good muon" consisted of at least two visible sparks in at least each of chambers 1 through 5, in both the direct and stereo views. These sparks were required to define a straight line in the direct view of chambers 1 and 2 and another straight line in the direct view of chambers 3 and 4. The two straight lines were required to intersect within the boundaries of the large magnet. Well over 95% of the muons left clear, well-defined straight lines of sparks in the entire array of chambers 1 and 2 and 3 through 8 making identification trivial. A straight line continuation beyond chamber 4 was not required to allow for multiple scattering in the shielding. No tracks were required beyond chamber 5 in order to allow for muons which exited the top or sides of the spectrometer. The computer program later identified

events which stopped in the spectrometer as pions. The "good muon" was also required to have the centers of the set of sparks, in each of chambers 1 through 4, define a straight line in the stereo view. This characteristic straight trajectory in the horizontal plane simplified the matching of tracks on opposite sides of the magnet.

Following these rules the scanners found approximately one measurable event for each three frames in the early data. Reflecting the improvement in the accidental rate, the later data had a two in three ratio. All of the film was scanned twice and much of it three times. The overall scanning efficiency was found by comparisons to be 99%.

B. Measuring and Reconstruction

Frames that were scanned as "good muons" were then measured on SLAC's Vanguard or NRI film plane digitizing machines. The Vanguard has a least count of 2.54 μ and punches its measurements on IBM cards. The NRI, a newer system, has a least count of 1 μ and outputs onto 7-track magnetic tape. On each frame the scanners measured the three principal fiducials and the muon track in both direct and stereo views. They were instructed to digitize as many sparks as they could, up to four, in each of chambers 1 through 4, and two sparks apiece in the remaining chambers. In the great majority of cases the chambers had more than 4 sparks and the maximum number were measured. We found the scanners measured points to within 14 μ on the Vanguard and 12 μ on the NRI. These correspond to 1.0 mm and .85 mm respectively, in real space.

Some 5% of the "good muon" frames contained two or more tracks (one of which was always a beam particle that had come through a veto). In such cases

both tracks were measured and the triggering particle selected by the programs later in the analysis.

The full set of dc fiducials, measured at the beginning of the rolls, provided a set of optical constants necessary to reconstruct spatial spark locations from their film plane coordinates. The three fiducials from each measurement were fit to the known fiducial locations which enabled correction for translation, rotation and magnification. The chi-square from this fit and the deviation from the average magnification in the fiducial plane (.013870) provide two indicators of the quality of measurement. A third, and the principle, indicator was provided by the fitting of the muon track through the 54" magnet field. In order to measure a momentum one must know the magnet's field and have three of the following four pieces of information: a point on the entering trajectory, a point on the exit trajectory, the slope of the entering trajectory, and the slope of the exit trajectory. Our situation is over determined since we have all four. All things being equally well measured we chose to insist that the final trajectory pass through each of the points and make an equal angular difference with each of the measured slopes. We called this angular difference the twitch angle (ϕ_y). This quantity clearly discriminated against mismatched pairs of tracks in the chambers before and after the magnet, as well as providing a sensitive measure of individual scanner and measuring machine performance. A similar technique was applied to the stereo images of the tracks in chambers 1 through 4 in order to eliminate mismatches in the stereo view (ϕ_z).

Events which failed to reconstruct properly (missing a fiducial or chamber view, etc.) and those events which exceeded the limits recorded in Table IV were remeasured along with any events on the scan list tapes found missing

from the reconstruction output. (The limits in Table IV were arrived at after study of the distributions.) After two complete measuring passes, and a partial third pass, efficiencies were computed from comparisons for each roll separately and applied to the roll normalization as a correction. The overall measuring efficiency was 98%.

C. Cuts

Of the events selected as "good muons" there were a sizable number that were not the results of a μ-p scattering. These could have been eliminated on a statistical basis by subtracting the normalized target empty events. We chose however to eliminate as many nonphysics events as possible by cuts in our SUMX programs before the target empty subtraction so as to minimize statistical variations. In addition, events were cut which could not be used for cross sections.

The cuts imposed, in addition to the requirements for a "good measurement" in Table IV were:

1. Radius cut. The minimum extrapolated distance (of the muon track) from the nominal beam line, within the 2-m length of the hydrogen target was required to be less than 7 cm. The typical full and empty radius distributions of Fig. 11 show a clear distinction between off beam line muons that cheat the veto system and target scatterings. This cut was the principal eliminator of frames triggered by halo muons. In the case of two muon tracks in a single photograph, the track with the smaller target radius was chosen as the triggering particle. In no case did both tracks have less than a 7 cm radius.

2. Geometric efficiency. Those events outside the range of well understood geometrical efficiency in p or θ were eliminated. This area and the bins

for which we give data are illustrated in Fig. 12. The principal event eliminators among these boundaries were the low angle cutoffs.

3. Fiducial volume. The muon tracks were traced through the spectrometer in a SUMX subroutine and were required to pass through the conservatively drawn active areas of the first five spark chambers and the three counter planes.

These criteria were applied to both target full and target empty events.

D. Elastic Events

As previously mentioned our apparatus was sensitive to the recoil proton from elastic μ-p scatterings as well as the elastically scattered muon. While we do not yet have elastic cross sections, we have over 2000 elastic events with protons. These elastic events were measured in a separate measuring pass using a list consisting of all frames which passed the criteria detailed above and had $K \leq 2.0$ GeV ($K=0$ for a perfect elastic event). The muon track was measured again in addition to any straight string of four or more sparks in both the direct and stereo views of the recoil chambers. Up to nine proton candidates could be measured in a frame. This proton requirement was loose and was generously interpreted so that many knock-on electrons were measured, and virtually every frame on the list was measured. In most cases proton tracks were easily distinguished, being long, straight and dark, but to be cautious two complete measuring passes were made through most of the 12 GeV data.

From this set of measurements we chose a sample of elastic events. Our aim in this regard was not to select all the valid events but merely an unbiased sample for use in the inelastic analysis. This selection was based on three parameters, in addition to the usual requirements on the muon. The

parameters were:

1. The minimum distance between the extrapolated muon and proton tracks.
2. The coplanarity angle of the elastic event.

$$\phi = \sin^{-1} \frac{(\vec{p}'_{\mu} \times \vec{p}'_{\text{proton}}) \cdot \vec{p}_{\mu}}{|\vec{p}'_{\mu} \times \vec{p}'_{\text{proton}}| \, |\vec{p}_{\mu}|}$$

3. A χ^2 fit to the elastic kinematics.

For future use we note that measurements in which only the muon was measured are called single arm measurements. Measurements in which both the muon and proton were measured are called double arm measurements.

E. Resolution

The angular resolution of the experiment was dominated by the angular distribution of the beam (illustrated in Figs. 8 and 9). To this was added in quadrature a measurement resolution of ± .7 mrad, determined by comparison of the 22,000 measurements of elastic candidates with their original single arm measurements. The resultant root mean square uncertainty in the scattering angle was ± 4.5 mrad.

The root mean square momentum resolution was found, by comparison of the single and double arm measurements, to be ± 200 MeV/c at 11.9 GeV/c. This corresponds to a $\frac{\Delta p}{p}$ of ± 1.7%.

Studies of the effects of these resolutions on the distributions of events in the K and q^2 bins showed individual bin "slopping" effects to be smaller than the stated statistical errors. Accordingly no corrections have been made to the data, but we have included a ± 1/2% uncertainty in our estimation of systematic error from this source.

F. The Beam Momentum

The elastic event measurements were used to check the nominal beam momentum values by reconstructing the quantity $E_0 = E' + q^2/2M_p$ for events passing the elastic requirements. Comparison of this distribution for the two elastic measuring passes, and then comparison of the several measurements of the same events, revealed small systematic differences between different measuring machines. These systematic errors caused differences in scattering angle as large as 0.3 mrad and differences in measured momentum as large as 70 MeV/c.

In order to minimize the error in V, we have calculated a central beam momentum for each processing block individually. Using "tight" cuts on the three elastic criteria we chose samples of elastic events from the double arm measuring passes. Then using the same frame numbers we compiled beam momentum distributions ($E_0 = E' + q^2/2M$) from the single arm measurements for each block. The beam momenta selected in this way ranged from $11.900 \pm .020$ (GeV/c) to $11.970 \pm .014$ (GeV/c) (the errors are statistical).

We estimate these numbers to be accurate to better than $\pm .030$ (GeV/c). Varying the beam momentum by this amount was found to change the measured cross section by $\pm 1.2\%$ in the overall normalization while having negligible effect on the q^2 variation.

G. Corrections

1. Geometrical Efficiency

The angular acceptance, or geometrical efficiency of the muon spectrometer was computed by a Monte Carlo technique computer program called Vegas. Vegas required as input data the outgoing muon momentum and scattering angle for which an efficiency was to be calculated. It chose randomly

the point of scatter within the target, the azimuthal angle of scatter, and a set of phase space coordinates H, θ_H, V, θ_V, constrained to be within the phase space area of the real beam. Using these parameters the program created a "muon" of known momentum, initial position, and observed scattering angle, and then traced its trajectory through the apparatus using the same magnet field routines as were used on the real events. The program then tested whether the trajectory hit the pole faces of the sweep or large magnets and if it passed through the active areas of the three trigger planes and first five spark chambers. The output of Vegas was the ratio of the number of events which pass these tests to the total number of events generated, which is the geometrical efficiency.

There were three versions of Vegas corresponding to the three trigger configurations used. Each generated a table of geometric efficiencies in p and θ which were used in the SUMX analysis programs. Figure 13 shows a smoothed plot of geometric efficiency as a function of scattering angle for different final momentum for the A2B2C1 trigger condition. In SUMX each event was weighted by the geometric efficiency appropriate to its individual kinematics. We have studied the sensitivity of the geometric efficiency to variations of the beam phase space of a magnitude which might not have been noticed. We present data in this paper only for those kinematic regions where such variations would cause less than 1/2% changes of the geometric efficiency itself. This is the origin of the low angle boundaries indicated in Fig. 12.

2. Radiative Corrections

The purpose of this experiment was to measure muon-proton inelastic scattering in such a fashion as to yield information about the muon-electron

difference and the interaction of virtual photons with protons. The most convenient quantity for these purposes is the cross section due to the simple one photon exchange diagram M1 in Fig. 14. What is actually measured, however, is this one photon exchange cross section plus a number of second order electromagnetic processes. These processes, shown to order α^3 in Fig. 14, introduce sizable, though well understood, differences in the observed cross sections of electrons vs. muons. The procedures for extracting the desired information are called the radiative corrections.

The problem is conventionally broken into two parts: 1) The radiative tails, which involve the emission of high energy photons. That is principally diagrams M7 and M8 (M9 and M10 are negligible in our case and were not calculated) and 2) The diagrams involving low energy photons (less than a few hundred MeV), which includes all the diagrams M2 through M10.

Most of the contributions of the second group of diagrams can be shown to cancel each other or to be negligible. What remains is the Schwinger correction,[31] δ, which contains the vertex and vacuum polarization corrections as well as various soft photon terms from M7 through M10. The effect of this second group of diagrams is to multiply the one photon exchange contribution by a factor $(1 + \delta)$. This correction, integrated over each of our bins and divided by bin size, is usually $\sim 2.5\%$ and never greater than 4%. ΔE was varied from 50 to 300 MeV with negligible effect on the correction.

The radiative tail diagrams, M7 and M8 have been calculated following the exact methods of Tsai.[32] In order to do this one must in principle know the inelastic cross sections. Since we did not have this precise knowledge, we divided the problem into three parts and made approximations.

The first part was the radiative tail of the elastic peak; these are diagrams M7 and M8 in which the proton remains a proton. For this part we used the proton elastic form factors. The largest correction stemmed from this source and is accurate to 2% of the correction.

The second part was the radiative tail of the N*(1236) resonances. This is the contribution of M7 and M8 in which the outgoing hadron is the N*. This contribution was calculated using a zero width approximation of the resonance after Mo and Tsai,[33] using form factors by Dufner and Tsai.[34,35,36]

The third part was the radiative tail of the "continuum" which represents the contributions of all the remaining resonances as well as the nonresonant background. For this we assumed

$$(\sigma_T + \epsilon\sigma_L) = 130\ \mu b/(1 + .8|q^2|)^2 ,$$

which was good enough since the correction was usually less than 3%.

According to this prescription the actual measured cross sections are then

$$\frac{d^2\sigma}{d\Omega dE_p} = \Gamma_T(\sigma_T + \epsilon\sigma_L)\,[1+\delta] + \left.\frac{d^2\sigma}{d\Omega dE_p}\right|_{\text{elastic tail}}$$

$$+ \left.\frac{d^2\sigma}{d\Omega dE_p}\right|_{N^* \text{ tail}} + \int_{E_p}^{E_{p\,max}} \frac{d^2\sigma}{d\Omega dE_p}(E'_p)\,dE'_p \quad .$$

The total radiative corrections written as the percentage by which the measured cross section was reduced is given in Table V under the title (Δ rad). We estimate their accuracy to be better than 10% of the correction in all cases. Further in the kinematic region of largest radiative correction (high K, low q^2), the contribution is nearly all due to the elastic radiative tail, which is accurate to 2% of the correction.

3. Small Corrections

In addition to the two major corrections above, there were a number of minor corrections which are listed below.

Spark chamber efficiency. A special scan was conducted of a large sample of film, selected at a regular interval through the data, to determine the loss of events due to the requirement of a minimum of 2 sparks per spark chamber. This investigation indicated a 1% ± 1/4% overall correction. Searches for other spark chamber inefficiencies, such as several chambers not firing, showed null results.

Pions. All events which had proper tracks in the first five chambers were measured. In the SUMX analysis program all events which stopped inside the steel or thick plate chambers downstream of chamber 5 were called pions. Approximately 150 events, concentrated in the two highest K bins, were rejected in this way.

Energy loss in target. Both the beam momentum and the outgoing muon momentum were corrected for energy loss due to ionization in the liquid hydrogen and in the target walls.

Electronics. As already mentioned, the dead time corrections to the normalization systems were 3-1/2% for the low current beam telescope and ~ 3% for the high current Bellamy monitor.

In addition we have made a 1% correction to the normalization for inefficiency in the trigger circuits.

Target empty. We took one half roll of events with the target empty, after every three rolls with the target full. This resulted in 89 acceptable events for $.5 \times 10^{10}$ incident muons. Target empty and target full cross sections were compiled separately and subtracted just prior to the radiative corrections. The subtraction was primarily in the low q^2, low K bins; the actual number of events in each bin is shown in Table V.

Film loss. A correction was made to the normalization of each roll for the number of frames which could not be measured. Included in this group were, the test strip frames cut from the ends of rolls for immediate development during the data taking, and badly developed or overexposed film. The overall magnitude of this correction was 2%.

H. Errors

In addition to statistical errors the data is subject to uncertainties from a number of sources. Some of these uncertainties simply affect the absolute normalization. The principal such error sources and their estimated root mean square contributions to the normalization error are

1.	Dead time in D2E4 (low current normalization)	$\pm \frac{1}{2}\%$
2.	Dead time in the high current beam monitor	$\pm \frac{1}{2}\%$
3.	Changes in beam shape and location between high and low current beams during the runs and adjacent normalizations	$\pm 1\%$

4. Spark chamber inefficiency $\pm \frac{1}{4}\%$

5. Scanning, measuring and processing $\pm \frac{1}{2}\%$

The rest of the errors are more complicated as they vary over the K, q^2 plane. The errors given below are root mean square errors, assuming the error distribution is gaussian.

Geometrical efficiency. The primary uncertainty in the Monte Carlo is due to the small uncertainty in the beam position and mean angle. It reflects itself mainly in the angular region below 60 mrad, corresponding to the low q^2 bins, where the effect can be as large as ± 1/2%: At higher angles the uncertainty is smaller than $\frac{1}{2}\%$ for all momenta.

Radiative corrections. This uncertainty varies with the size of the radiative correction. It introduces less than ± 1/2% error in the overall normalization.

Resolution. The incorrect placement of events in bins due to the resolution in momentum and angle, contributes a ± 1/2% uncertainty.

Momentum. The measuring machine differences produced a ± 50 MeV/c uncertainty in the momentum of the outgoing muon. Since the beam momentum is determined from these measurements there must be a similar error in it. Variation of both the scattered muon and beam momentum by this amount resulted in an overall normalization uncertainty of ± 1%, the effect being greatest in the low K bins.

Angle. The comparison of several measurements of the same events left us with a possible ± .3 mrad angular uncertainty. Increasing the angle of all the data events by this amount and recompiling cross sections showed an overall increase in cross section of .9% evenly spread over the K, q^2 plane.

Beam momentum. Aside from the uncertainty in measured momentum we believe we have determined the beam momentum, relative to the inelastic measurements of each block, to approximately ± 15 MeV/c. Variation of the input beam momentum in the analysis programs and recompiling the cross sections we found the overall normalization to change by ∓.6%. The effect was greatest in the low K, low q^2 bins (2% at the extreme) but negligible over most of the plane.

Internal consistency. We now face an old dilemma in experimental physics, how to combine these systematic errors. The usual choices are adding in quadrature, which gives 2%, or simple addition, which results in ±6%. We do have one guide to the magnitude of the systematic error of the experiment, and that is its internal consistency.

As previously mentioned the data was divided into six processing blocks according to time and trigger conditions. Comparison of these blocks showed excellent agreement, with one exception. The three highest K bins of block 2A were lower than the rest of the data. (This block had an A3B3C2 trigger and was run at the end of the experiment's early running cycle. It represents 12.6% of the incident flux.) Further investigation indicated a possible decrease with time within the block. The most likely source of such a problem would be a malfunctioning C plane trigger counter group. Unfortunately no significant corroborating evidence was found from scatter plots or scaler information. Accordingly we have left block 2A in the data. In terms of a single parameter normalization fit, inclusion of block 2A lowers the cross section by 1%. Looking only at the three highest K bins, inclusion of 2A causes a normalization fit decrease of 2.5%.

Comparisons were also made between the low statistics data taken with a 10 GeV/c beam[6] and the 12 GeV/c data reported here, in their regions of kinematic overlap. This study indicated that the 10 GeV/c data was generally higher in cross section than the 12 GeV/c data. A simple one parameter normalization fit gave the difference as $9.0 \pm 6.0\%$.

We do not consider this discrepancy to be very significant. It could clearly be statistical fluctuation. In addition the 10 GeV/c data was the earliest stage of the experiment and many improvements in the experiment and analysis had been subsequently made. Many of the checks on the 12 GeV/c data were not done for the 10 GeV/c; no elastic measurements were made; the 10 GeV/c beam was not directly measured; and the 54" magnet field was monitored only by a shunt of questionable integrity. None the less, the authors feel sufficiently cautioned to prefer the conservative method of combining systematic errors. We therefore ask that a $\pm 6\%$ systematic uncertainty, beyond statistical error, be attached to our data.

VI. RESULTS

The data is shown in Table V, all errors listed are statistical and do not include the ± 6% maximum systematic error. K bins were chosen to facilitate the comparison to the electron data. A lower bound at K=.6 (missing mass = 1415 MeV) was set in order to avoid contamination by elastic events. The limit at the $|q^2|$ of 4 $(GeV/c)^2$ in the low K bins is due to the small size of the cross section while all the other boundaries are imposed by the geometrical efficiency.

As previously mentioned we are unable to separate σ_T and σ_S so the virtual photon total cross section is given in terms of the combination σ_{exp} where

$$\sigma_{exp,\mu}(q^2, K, p) = \sigma_T(q^2, K) + \epsilon(q^2, K, p, m_\mu)\, \sigma_S(q^2, K) \quad . \tag{34}$$

We have also listed the values of ϵ appropriate to the center of each bin. The values of $\sigma_{exp,\mu}$ shown in the table are not directly derivable from the listed values of $d^2\sigma_\mu/dq^2dk$ because in the compilation of $\sigma_{exp,\mu}$ each event is weighted by the inverse of its particular Γ_T.

We observe $\sigma_{exp,\mu}$ to show the same qualitative behavior with q^2 and K as we observed in our 10 GeV/c results and as seen in the extensive electron-proton inelastic measurements from SLAC.[37] Our data exhibits particularly well the smooth falloff with $|q^2|$ from the photoproduction measurements at $|q^2|=0$ (Fig. 17). At higher $|q^2|$ values σ_{exp} decreases as fast or faster than $1/|q^2|$ but not as fast as $(1/|q^2|)^2$. This mild $|q^2|$ behavior is widely considered to be evidence for the point-like constituent internal structure of the proton.[38]

As explained previously σ_T and σ_S are only one of an infinite set of possible pairs of empirical structure functions. The other pair which is of

current interest is W_1 and W_2, defined in Eqs. (29) and (30). It has been suggested by Bjorken and others[38] that at large values of ν and q^2 the product νW_2 might be a function of only the combination $x = |q^2|/2M\nu$. This prediction, which is commonly called scaling has been generally confirmed by the electron-proton inelastic scattering experiments. We have listed in Table V our values of x and νW_2 as computed using the central K and $|q^2|$ in each bin and assuming an R of .18.[39] This data is plotted in Fig. 15.

VII. THE MUON-ELECTRON COMPARISON

In comparing muon-proton and electron-proton inelastic scattering, one must establish that known effects would not produce a difference. Lowest order weak interaction effects can be excluded on the basis of the small coupling constant and their equality for the muon and electron. The contributions of some higher order electromagnetic diagrams have been excluded by the radiative corrections to both the muon and electron data. (It should be pointed out, however, that these procedures depend upon the validity of quantum electrodynamics.) No correction has been made for the two photon exchange contribution to inelastic scattering, Fig. 3. This two photon exchange diagram could produce a muon-electron difference because such a term is sign dependent and we are comparing positive muons to negative electrons. But as discussed in Section III.B, there is evidence that two photon exchange in inelastic scattering is at most a few percent effect. Therefore we ignore this effect in our considerations.

A. The Method

In making this comparison between muon and electron cross sections we must consider three kinematic effects. First, the quantity we are using, $\sigma_{exp,\ell}$ depends, through the quantity ϵ, on the incident lepton momentum, which was different for the two experiments. It also depends very weakly on the lepton mass. Second, the muon data was acquired over a continuous area of the K, q^2 plane; the electron data on the other hand was taken at discrete points along straight lines in the plane. And third, the muon data extends to a lower q^2 than the published electron data from SLAC.[37]

To allow for the first of these effects we have modified each of the electron data points through the equation

$$\sigma_{exp,e}(q^2,K,p_\mu) = \left\{\frac{1+\epsilon_\mu(q^2,K,p_\mu,m_\mu)\,R(q^2,K)}{1+\epsilon_e(q^2,K,p_e,m_e)\,R(q^2,K)}\right\}\sigma_{exp,e}(q^2,K,p_e) \quad , \tag{35}$$

$$= F(q^2,K,p_\mu,p_e,m_e,m_\mu)\;\sigma_{exp,e}(q^2,K,p_e)$$

where

$$R(q^2,K) = \sigma_S(q^2,K)/\sigma_T(q^2,K) \quad .$$

In this way the electron data appears to have been taken with a 12 GeV/c incident beam and with particles of the muon's mass. This procedure is, however, subject to error due to the uncertainty in the value of R. At $q^2=0$ R must equal zero. Aside from this, knowledge of R is confined to measurements at only a few values of q^2, K in the region of this experiment. These measurements are consistent with R=.18 or with $R=|q^2|/16$. Fortunately for our comparison, ϵ is a slow function of beam momentum and lepton mass, and the factor F is rather insensitive to the value chosen for R. Specifically,

$$\Delta F = \left(\frac{\epsilon_\mu - \epsilon_e}{(1+\epsilon_e R)}\right)\Delta R \quad . \tag{36}$$

Even if R=1±1, the uncertainty in $\sigma_{exp,e}$ is for the most part less than 1%. We have made the complete comparison assuming R=.18 and also with R=0, 1.0, and $|q^2|/16$. The changes in the fits and confidence levels, which are presented later, are negligible.

An understanding of the second effect is facilitated by reference to Fig. 16. The e-p inelastic experiment[37] detected the outgoing momentum spectrum

for a fixed angle and a fixed incident momentum. This choice of θ and E_0 defines a straight line in the K, q^2 plane given by:

$$K = E_0 - q^2 \left(\frac{1}{2M_p} + \frac{1}{4E_0 \sin^2 \theta/2} \right) \quad . \tag{37}$$

The electron data used for this comparison were taken at $\theta = 6^o$ and 10^o and over a range of incident energies indicated in Fig. 16. The data points on all the lines are very closely spaced from K=0 to K $\approx$ 2.4 GeV. Beyond that point they are widely separated but at almost the same K on all the lines.

The muon data on the other hand continuously covers the kinematic plane. The result quoted for a bin actually represents a double integral of the cross section in K and q^2 over the area of the bin. Within each K, q^2 bin we have assigned the muon data to have its central q^2 value. The problem then is to compile the electron cross sections in a way directly comparable to the muon data. To do this we have chosen the muon data K bins so that the high K bins bracket the single electron points while the two low K bins contain the continuous electron spectra. We then have made the segment of each "line" within a K bin into a single data point by integrating in K and compiling a weighted average q^2. In those cases in which there was only one point from a "line" in the K bin the point was taken as the integral in K and assigned its measured q^2 value. The electron data compiled in this way is presented in Table VI.

The last effect is that the muon data extends to lower q^2 values than does the 6^o and 10^o electron data. In order to make the comparison we have used the measured values of the $q^2 \rightarrow 0$ limit of σ_{exp}. This is $\sigma_{\gamma p}(K)$, the total cross section for the production of hadrons in the interaction of real photons

with protons. K is the energy of the photon in the laboratory system. We used values of $\sigma_{\gamma p}(K)$ from a fit to the photoproduction data from several labs.[40,41,42] These are listed in Table V and plotted on Fig. 17. The errors have been increased to ± 6% to allow for possible relative systematic errors between experiments.

In Fig. 17 $\sigma_{exp,\mu}(q^2,K,p_\mu)$, $\sigma_{exp,e}(q^2,K,p_\mu)$ and $\sigma_{\gamma p}(K)$ are shown as functions of q^2 for the various K intervals. It is obvious that any possible muon-electron differences are small. To quantify those differences we must extrapolate one set of points to the same q^2 values as the other set. We do this by making a fit to the γ-p and electron points in each K bin. The only criterion for these fits was how closely they reproduced the input data points with a smooth curve. Adding the six fits we have a χ^2 of 20.09 for 46 points (28 degrees of freedom). The fits are intentionally overparameterized and we ascribe no physical meaning to them.

We then define the ratio:

$$\rho(q^2,K,p_\mu) = \sigma_{exp,\mu}(q^2,K,p_\mu)/\sigma_{exp,e,Fit}(q^2,K,p_\mu) \qquad (38)$$

at the q^2, and K points of the muon data. This ratio is listed in Table VI and plotted in Fig. 17. The errors shown are the combined statistical errors only. In addition to these, the muon data has a conservative ± 6% systematic error, while the electron data is quoted with a ± 5% systematic uncertainty. Thus the combined overall normalization uncertainty (excluding statistical errors) in the comparison is ± 8% if the two uncertainties are added in quadrature.

B. Conventional Analysis

We see from Fig. 17 that $\rho_{inelastic}$ is close to 1.00; if there is an effect the muon data appears to be lower. To be quantitative we need a model of how

the two sets of measurements might differ. The most obvious possibility is that there is a relative normalization error between the experiments. To investigate this we have fit all of the $\rho_{\text{inelastic}}$ points to a single parameter $\rho_{\text{inelastic}} = N^2$ where N^2 is a constant. (In order to eliminate any effect arising from distortion in the $\sigma_{\gamma p}$, $\sigma_{\text{exp, e}}$ fit we have also made a single parameter fit to the ratio of the electron data points of Table VI to the fit. The result we present for N^2 is actually the ratio of N^2_μ from the muon points to N^2_e from the electron points. The statistical errors quoted are the quadratic sum of both fits, but the chi-square is from the muon fit only. A similar procedure has been followed for all the fits given in this paper.) We find

$$\rho_{\text{inelastic}}(q^2, K, 12\ \text{GeV/c}) = N^2 = .917 \pm .024 \qquad (39)$$

with $\chi^2 = 42.1$ for 43 degrees of freedom. The error is statistical only. To this must be added the ± 8% normalization uncertainty. We note that this simple form gives an excellent fit, a point to which we will return later. We also note that, given the size of the systematic error, $\rho_{\text{inelastic}}$ is consistent with 1.00.

A more interesting approach to the analysis is to suppose that the result of our comparison is rooted in basic physics. As discussed in Sections II.B and III, the leptons can be assigned the inelastic form factor $G'_\ell(q^2, K)$ and the elastic form factor $G_\ell(q^2)$. As also discussed in these sections, there is little theoretical guidance as to what such a lepton form factors should look like.[7] We know only that $G'_\ell(q^2=0,\ K=0) = 1.0$, and that $G_\ell(q^2=0) = 1.0$.

To simplify the analysis we assume that the inelastic form factor

$$G'_\ell(q^2, K) = 1/\left[1 + |q^2|/\Lambda'^2_\ell\right] \quad . \qquad (40)$$

Thus we take G'_ℓ to be independent of K or to have already averaged over K. Λ'_ℓ is not necessarily the same as Λ_ℓ in Eq. (15). (The parameters associated with inelastic scattering are primed to distinguish them from the analogous elastic parameters.) We may also take Λ'_ℓ to be an inverse measure of the deviation of the lepton from a point particle. For very small $|q^2|$, namely for $|q^2| \ll m_\ell^2$ we may use the nonrelativistic interpretation of Eq. (16)

$$\Lambda'^2_\ell = 6/\langle r'^2_\ell \rangle \quad .$$

Then

$$\rho_{\text{inelastic}}(q^2, K, 12\ \text{GeV/c}) = \sigma_{\text{exp},\mu}(q^2, K, p_\mu)/\sigma_{\text{exp},e}(q^2, K, p_\mu)$$

$$= \frac{\left(1 + |q^2|/\Lambda'^2_\mu\right)^{-2}}{\left(1 + |q^2|/\Lambda'^2_e\right)^{-2}} \quad . \tag{41a}$$

To order $|q^2|$ Eq. (41a) becomes

$$\rho_{\text{inelastic}}(q^2, K, 12\ \text{GeV/c}) = 1/\left[1 + |q^2|/\Lambda'^2_D\right]^2 \tag{41b}$$

where

$$\Lambda'^{-2}_D = \Lambda'^{-2}_\mu - \Lambda'^{-2}_e \quad .$$

In the nonrelativistic limit

$$\Lambda'^{-2}_D = \frac{1}{6}\left(\langle r'^2_\mu \rangle - \langle r'^2_e \rangle\right) \quad . \tag{42}$$

We have made a fit to this form for the points in all the K bins. The result is

$$\Lambda'^{-2}_D = .049 \pm .012\ (\text{GeV/c})^{-2} \tag{43}$$

with $\chi^2 = 44.3$ for 43 degrees of freedom.

Because this comparison used data from two different experiments one might insert another parameter, N'^2, to allow for a normalization difference. Generalizing Eq. (41b)

$$\sigma_{\text{inelastic}}(q^2, K, 12\ \text{GeV/c}) = N'^2/\left[1+|q^2|/\Lambda_D'^2\right]^2 \quad . \tag{44}$$

Fitting to this form we find:

$$N'^2 = .946 \pm .042, \quad \Lambda_D'^{-2} = .021 \pm .021\ (\text{GeV/c})^{-2} \tag{45}$$

with $\chi^2 = 41.1$ for 42 degrees of freedom.

These statistical errors are somewhat misleading because they are correlated. A more accurate description is given by Fig. 18. This plot displays the one and two standard deviation ellipsis based on statistical errors only. The ± 8% relative normalization uncertainty is not included, its effect is to allow the N^2 scale to be shifted up and down by an amount as large as 0.08. These results mean that the muon-proton inelastic cross section falls off very slightly faster with $|q^2|$ than the electron cross section, but that this $|q^2|$ variation is not statistically significant. And once again, given the size of the systematic uncertainty it is quite possible that $N'^2 = 1$ and $\Lambda_D'^{-2} = 0$ and that there is no muon-electron difference.

Reflection on the results of the three fits discussed above, as well as a number of others, has led the authors to two conclusions. First, there is no statistically significant evidence for any q^2 dependence. A normalization type difference is favored. And second, the ± 8% systematic uncertainty precludes establishing any muon-electron difference.

There is however, one piece of information that can be extracted. From the fit to Eq. (44) we can establish a lower limit on Λ_D'. With 97.7% confidence

$$\Lambda_D' > 4.1\ (\text{GeV/c}) \quad .$$

Though we are certainly outside the nonrelativistic realm of applicability of Eq. (42) it is conventional to phrase this number as a limit on the difference in size between the muon and electron. We find

$$\langle r'^2_\mu \rangle - \langle r'^2_e \rangle < (1.2 \times 10^{-14} \text{ cm})^2 \quad .$$

All of the foregoing analysis is based on the assumption that G'_ℓ is a function of only q^2. Another possibility at the other extreme is that G'_ℓ is a function of only K. We have investigated this by fitting to the simple form:

$$\rho_{\text{inelastic}}(q^2, K, 12 \text{ GeV/c}) = (C + DK)^2 \quad , \tag{46}$$

the best fit was

$$C = .960 \pm .017 \qquad D = .000 \pm .003 \qquad (\text{GeV/c})^{-1} \quad .$$

We conclude that our experiment indicates no K dependence. We also conclude that there is no point in making G'_ℓ a function of both q^2 and K.

C. Comparison with other Experiments

There are no other muon-proton inelastic scattering experiments to which this one may be directly compared. There have been however two muon-proton elastic scattering experiments[2,3] which probe the muon-virtual photon vertex in a way similar to ours. In order to make a comparison with electron-proton elastic scattering experiments they make the assumption $G_M(q^2) = 2.79\, G_E(q^2)$ in the Rosenbluth formula (Eq. (12)). If the lepton is assigned the elastic form factor $G_\ell(q^2)$, the combination $\left[G^2_M(q^2)\, G_\ell(q^2)\right]$ can then be extracted from the differential cross section $(d\sigma/d\Omega)_{\ell p,\ \text{elastic}}$.

In analogy to $\rho_{\text{inelastic}}$ we define

$$\rho_{\text{elastic}}(q^2) = \frac{\left[G_M^2(q^2)\, G_\mu^2(q^2) \right] \mu p, \text{elastic}}{\left[G_M^2(q^2)\, G_e^2(q^2) \right] ep, \text{elastic}}$$

$$= G_\mu^2 (q^2)/G_e^2 (q^2) \qquad (47)$$

The values of ρ_{elastic} from the experiments of Camilleri et al.,[2] are shown in Fig. 19. Here too, the ratio appears to be less than one. A one parameter fit, $\rho_{\text{elastic}}(q^2) = N^2$, gives

$$N^2 = .922 \pm .013 \qquad (48)$$

as the best fit. Adopting the conventional form factor Eq. (15b) and an experimental normalization correction term N^2, they also fit their data with

$$\rho_{\text{elastic}}(q^2) = \frac{N^2}{\left(1+q^2/\Lambda_D^2\right)^2} \quad . \qquad (49)$$

Camilleri et al. give as a best fit

$$N^2 = .953 \pm .033 \qquad \Lambda_D^{-2} = .064 \pm .056\ (\text{GeV/c})^{-2} \ . \qquad (50)$$

This group estimates their systematic error as 4.5% and the systematic error in the electron data as 1 - 2%. With 95% confidence they give a lower limit of

$$\Lambda_D > 2.4\ \text{GeV/c} \quad . \qquad (51)$$

The earlier experiment of Ellsworth et al. was analyzed in a slightly different manner. These authors presented results for Eq. (49) with N^2 set

at 1.0 and also with N^2 set at .80. For N^2=1.0, Λ_D^{-2}=0.172±.033 $(GeV/c)^{-2}$ with a χ^2=17 for 9 degrees of freedom. Dropping one bad point the fit becomes N^2=1, Λ_D^{-2}=.009±.032 (GeV/c) with a χ^2=3.6 for 8 degrees of freedom. Finally for N^2=.80, Λ_D^{-2}=0±.033 $(GeV/c)^{-2}$. And based on the first N^2=1 fit, Λ_D > 2.04 GeV/c with 95% confidence.

We find our results in surprisingly good agreement with these two experiments. Neither experiment gives statistical evidence of a q^2 variation, while both $\rho_{inelastic}$ and $\rho_{elastic}$ are on the average less than 1.0. But, as we have already noted, there is no required relationship between the pair of parameters N', Λ_D', and the pair N, Λ_D. And, once again, the finding that both N' and N give best fits when less than 1.0 might be attributable to systematic experimental error. We shall discuss this further in Section VIII.

There are no other experiments which explicitly measure the difference parameter Λ_D. There are though, a number of experiments which are sensitive to the individual lepton form factors and can be compared to theoretical calculations. These yield values of either Λ_μ or Λ_e. Principle among them is the muon g-2 experiment.[24] As discussed in Section II.D this measurement agrees with the predictions of quantum electrodynamics to a very high precision, and consequently imposes a strong constraint on the hypothetical lepton form factor. The modification to a_μ^{theory} due to the inclusion of the form factor of Eq. (15a) at each real muon vertex has been calculated.[19] The modification may be expressed as multiplication of a_μ by the factor

$$1 - (4/3)\left(m_\mu^2/\Lambda_\mu^{g2}\right) \tag{52}$$

Then with 95% confidence[24]

$$\Lambda^g > 7.0 \text{ GeV/c} \quad . \tag{53}$$

We note that while lepton-proton inelastic and elastic scattering involves only spacelike values of q^2, the calculation of the limit on Λ_μ^g involves both spacelike and timelike values of q^2.

Restrictions on the muon form factor for timelike values of q^2 have been obtained[43, 44, 45] by studying the electron-position colliding beam process

$$e^- + e^+ \rightarrow \mu^- + \mu^+ \quad . \tag{54}$$

We find that the result of V. Alles Borelli et al.[43] gives approximately the restriction

$$\Lambda_\mu^c > 6.0 \text{ GeV/c} \tag{55}$$

with 95% confidence. Here the form factor of Eq. (15a) has been used. The superscript c on Λ_μ^c indicates that this is a colliding beam measurement. Thus the g_μ experiment and the colliding beam experiment, like the inelastic and elastic scattering experiments, find only lower limits on the Λ parameter in Eq. (15a).

We can extract a limit on Λ_μ' from Λ_D' if we make an assumption about the limits on Λ_e'. We assume that Λ_e' is the same as Λ_{ee}, where Λ_{ee} is the Λ parameter obtained by applying the form factor of Eq. (15a) to electron-electron elastic scattering,

$$e^- + e^- \rightarrow e^- + e^- \quad . \tag{56}$$

We distinguish Λ_{ee} from Λ_e, the Λ parameter measured in electron-proton elastic scattering, because Λ_e might show the effect of an unknown electron-hadron interaction.

The most restrictive limit on Λ_{ee} comes from the measurement[46] of electron-electron elastic scattering in electron-electron storage rings. Comparison of the experimental result with the Møller cross section,

modified by the inclusion of the form factors of Eq. (15a) at both lepton vertices, gives: $\Lambda_{ee}^{-2} \simeq -0.022 \pm 0.025\ (\mathrm{GeV/c})^{-2}$. If we insist that Λ_{ee}^{-2} be greater than zero, as the charge radius interpretation of Eq. (16) would require; we find

$$\Lambda_{ee} > 6.1\ (\mathrm{GeV/c}) \tag{57}$$

with 95% confidence. Combining this result with our result for Λ_D' we find

$$\Lambda_\mu' > 3.2\ \mathrm{GeV/c} \tag{58}$$

with 95% confidence.

VIII. SPECULATIONS

In our inelastic experiment and in the two elastic experiments, there are no statistically significant indications of any q^2 dependent differences between the muon and the proton. But, in all of these experiments the muon cross sections turn out to be lower than the electron cross sections. We emphasize that in our experiment this difference is not significant because the overall normalization uncertainty is about 8%. In the elastic experiments the authors give a smaller normalization uncertainty for the muon data, but the combined overall normalization uncertainty of the muon and electron data might be as large as our 8%. Thus the low muon cross section in any one experiment is not significant. However we should not totally ignore these "normalization differences." At the very least we should use them for hints as to what might be the most fruitful direction for future experiments on the muon-electron difference. The development of these hints, or perhaps better speculations, is the purpose of this section.[7]

If we look at the muon-proton inelastic and elastic experiments, with no preconceived notions as to how the muon-electron difference might behave with q^2 we would not use the form factors $1/\left[1+|q^2|/\Lambda_\ell^2\right]$. Instead we would use a form which gives a roughly q^2 <u>independent</u> difference between the muon and electron cross sections in the q^2 range covered by the experiments. We would of course also require $G_\ell(0)=1$. A simple example of such a model is one in which the electron is indeed a point Dirac particle so that $G_e(q^2)=1$, and

$$\begin{aligned} G_\mu(q^2) &= (1-b) + b/\left(1+|q^2|/\Lambda_\mu^2\right) \\ &= 1 - (b|q^2|)/\left(|q^2|+\Lambda_\mu^2\right) \qquad 0 \le b \le 1 \end{aligned} \tag{59}$$

Then in the scattering experiments as $|q^2|$ increases

$$\rho_{\text{inelastic}}(q^2, K) = \rho_{\text{elastic}}(q^2) \xrightarrow[|q^2|\to\infty]{} (1-b)^2 \quad .$$

Thus at high values of $|q^2|$ only a "normalization difference" would be observed. The form factor of Eq. (59) could come from the following model. Take the muon to have (1-b) of its electric charge concentrated in a point and b of its electric charge spread out in a halo of radius $\sqrt{6}/\Lambda_\mu$ (see Eq. (16)). To fit the "normalization differences" found in the inelastic and elastic experiments, b would have a value in the vicinity of .05. Thus this model may be described as a mostly point muon with a small fraction of the electric charge in a halo around the point.

Up to now we have been concerned with fitting a form factor to the high energy scattering experiments. But, as previously discussed, any such form factor modification would affect the value of the lepton gyromagnetic moment. Thus the result of Picasso et al.[24] imposes a limit on the parameters b and Λ_μ from Eq. 58. The g-2 experiment is essentially a low $|q^2|$ measurement, if we approximate Eqs. (59) and (15a) in this limit we find

$$b/\Lambda_\mu^2 \approx 1/\Lambda_\mu^{g^2} \quad .$$

So, by Eq. (53)

$$b/\Lambda_\mu^2 < .02 \text{ with } 95\% \text{ confidence} \quad .$$

Unfortunately this limit does not give very good agreement with the high energy scattering results as we can see by considering the region in which

$|q^2|/\Lambda_\mu^2 \ll 1$ where:

$$1 - \rho_{\text{inelastic}} = 1 - \rho_{\text{elastic}} \approx 2b|q^2|/\Lambda_\mu^2 < .04|q^2|$$

with 95% confidence. For $|q^2|$ values less than 1 the "normalization differences" are then limited to less than 4% with 95% confidence, which, while not inconsistent, is on the edge of compatability with the data. Thus the function given in Eq. (59) is not a very good choice for the muon form factor.

What is required is a form factor which is a more rapid function of q^2. An example of such an expression is

$$G_\ell(q^2) = 1 - b + b/\left(1 + (q^2)^2/\Lambda_\ell^4\right) \quad . \tag{60}$$

In the limit $(q^2)^2/\Lambda_\ell^4 \gg 1$, this form gives

$$G_\ell(q^2) \rightarrow 1 - b_\ell$$

and

$$\rho_{\text{inelastic}} = \rho_{\text{elastic}} \rightarrow \frac{(1 - b_\mu)^2}{(1 - b_e)^2} \quad . \tag{61}$$

So Eq. (61) would look like a normalization discrepancy. We have fit our data to this form assuming $b_e = 0$ and

$$b_\mu = .062 \pm .032 \qquad \Lambda_\mu^{-4} = 3.2 \pm 3.9 \ (\text{GeV/c})^{-4}$$

with $\chi^2 = 45.8$ for 42 degrees of freedom. Equation (60) with the parameters given above is consistent with the g_μ experiment[24] which led to the limit on Λ_μ^g given in Eq. (52). It is similarly consistent with the $e^+ + e^- \rightarrow \mu^+ + \mu^-$ experiment[43] which led to the limit on Λ_μ^c given in Eq. (55).

In the foregoing we have attempted to explain the various experimental data in terms of a muon form factor. An alternate approach, as discussed in Section II.C, is to postulate a special muon-hadron interaction. Such an interaction can conceivably explain the "normalization differences" in both the elastic and inelastic scattering experiments and yet have only very small effects on the gyromagnetic moment and the $e^+ + e^- \rightarrow \mu^+ + \mu^-$ cross section.

As shown in Fig. 20, we assume that the special muon-hadron interaction is mediated by a neutral particle X with mass M_x. Though it is not necessary to do so, we also assume that the X particle has spin 1. The coupling constants are indicated in the diagrams; e is the electric charge. The coupling constants at the lower vertices are to be regarded only as very crude measures of the strength of the coupling of the virtual photon or the X particle to hadrons. Muon-proton inelastic scattering would take place through the sum of the two diagrams in Fig. 20. The second diagram would result in a difference between muon-proton and electron-proton inelastic cross sections, because only the first diagram would enter in electron-proton inelastic scattering. Then, to lowest order in the coupling constants,

$$\rho_{\text{inelastic}}(q^2, K) = \left[1 + \left(\frac{f}{e}\right)\left(\frac{g_{xh}}{g_{\gamma h}}\right)\left(\frac{|q^2|}{|q^2| + M_x^2}\right)\right]^2 \quad . \qquad (62)$$

Taking $(f/e)\,(g_{xh}/g_{\gamma h})$ to be real and negative, the best fit of our data to this form gives

$$(f/e)(g_{xh}/g_{\gamma h}) = -.055 \pm .031 \qquad \text{and} \qquad M_x^2 = .184 \pm .443\ (\text{GeV}/c^2)^2 \qquad (63)$$

with $X^2 = 42.75$ for 42 degrees of freedom. The reader should be cautioned that this is only an example. The special muon-hadron interaction could involve many or all hadrons; and Eq. (62) and the fits in Eq. (63) would then just illustrate one of the simplest cases. In particular we do not mean to suggest that some undiscovered hadron of mass M_X is required for a special muon-hadron interaction.

A conventional speculation[21,22] is that the X particle is some undiscovered heavy photon with e=f. But we prefer the speculation that the X particle is itself a hadron. More generally the X particle might be taken to represent the summation of the interaction of different kinds of hadrons with the muon. To estimate the present experimental limits on f, the coupling of the muon to the hadron X, we take $(g_{xh}/g_{\gamma h})^2$ to be the ratio of a typical hadron-hadron total cross section (30 mb) to the photon-proton total cross section (0.12 mb). Our muon-proton inelastic scattering measurements indicate b to be approximately .05. Then

$$f/e \approx .05/\sqrt{250} \approx 1/300 \quad . \tag{64}$$

Thus in this "X=hadron" model, the coupling of the muon to the hadrons is much weaker than the electromagnetic coupling. If such a coupling does exist, it can most likely be found only through the study of muon-hadron reactions. It will be difficult to find in purely electromagnetic experiments because the enhancement factor $(g_{xh}/g_{\gamma h})$ will not be available.

As an example, we consider the effect of this "X-hadron" model on g_μ. The inclusion of X exchange in the g_μ calculation produces a modification

given by Kobzarev and Okun[21] as

$$\frac{\Delta g_\mu}{g_\mu} = \frac{1}{3\pi}\left(\frac{f^2}{M_X^2}\right) m_\mu^2$$

which combined with the results of Picasso et al.[24] gives

$$\frac{f^2}{M_X^2} = (2.5 \pm 2.9) \times 10^{-4}\ (\mathrm{GeV/c^2})^{-2}$$

or

$$\frac{f^2}{M_X^2} < 8.3 \times 10^{-4}\ (\mathrm{GeV/c^2})^{-2} \qquad (65)$$

with 95% confidence. Taking M_X^2 from Eq. (63) yields the limit

$$f/e < .15 \quad . \qquad (66)$$

Equation (66) gives an upper limit to f/e which is much larger than the speculative estimate given in Eq. (64). The precision of the g_μ experiment would have to be improved by at least a factor of 1000 to test the estimate given in Eq. (64). Not only is this precision unobtainable with present experimental methods, but an effect of this very small size will be completely obscured by the expected strong interaction contribution[11] to g_μ. Similar remarks hold for the contribution of the "X-hadron" model to the process $e^+ + e^- \rightarrow \mu^+ + \mu^-$. In the above we have assumed that the muon has a special interaction with hadrons and the electron is the conventional charged lepton with only electromagnetic and weak interactions. The contrary position can also be taken. There is a special electron-hadron interaction and the muon is the conventional charged lepton. The same analysis can then be pursued. The only difference

is that the effect of the "X-hadron" model in purely electromagnetic interactions is even smaller.

Of course, all of this is highly speculative. We have found no statistically significant violation of the principle of muon-electron universality, and the mu-e puzzle remains. But, the agreement between muon and electron scattering cross sections is not as good as we might hope for. A curious 8%, possibly systematic "normalization error", has persisted through three experiments and must yet be resolved. The results of this investigation seem to indicate that future experimenters might best seek to answer the question of muon-electron scattering differences by making high precision measurements at moderate values of $|q^2|$; rather than going to as high a $|q^2|$ as possible, as was done in this experiment. The challenge of this field will be to reduce the limits of systematic errors, in both muon and electron experiments, to a level at which a 5% difference will be unquestionably significant.

We wish to express our deep thanks to Professors H. C. Bryant, B. D. Dieterle, and E. H. Bellamy; and to Mr. J. C. Pratt for his assistance. We also wish to express our grateful thanks to our technicians and programmers and to the staff of the Accelerator Operations Group. We are deeply indebted to the scanners of the Conventional Data Analysis Group for their long and diligent labor. Finally we would like to acknowledge the kindness and help of the SLAC-MIT electron scattering collaboration for providing us with their extensive and precise data.

REFERENCES

1. W. T. Toner et al., Phys. Letters 36B, 251 (1971) is a brief report of the results presented in this paper.
2. L. Camilleri et al., Phys. Rev. Letters 23, 153 (1969).
   L. Camilleri, Columbia University Nevis Laboratories Report No. NEVIS-176 (1969), unpublished.
3. R. W. Ellsworth et al., Phys. Rev. 165, 1449 (1968).
4. J. Cox et al., Nucl. Instr. Methods 69, 77 (1969).
5. W. T. Toner in Proceedings of the 4th International Symposium on Electron and Photon Interactions at High Energy (Daresbury Nuclear Physics Laboratory, Daresbury, England, 1969).
6. B. D. Dieterle et al., Phys. Rev. Letters 23, 1187 (1969).
7. For a more complete discussion of the material contained in this section see M. L. Perl, Report No. SLAC-PUB-982 (1971), to be published in the Proceedings of the Muon Physics Conference (Colorado State University, Fort Collins, Colorado, 1971).
8. T. D. Lee and C. S. Wu, Ann. Rev. Nucl. Sci. 15, 381 (1965).
9. R. E. Marshak, Riazuddin and C. P. Ryan, Theory of Weak Interactions in Particle Physics (Wiley-Interscience, New York, 1969).
10. G. Feinberg and L. M. Lederman, Ann. Rev. Nucl. Sci. 13, 431 (1963).
11. S. J. Brodsky in Proceedings of the 4th International Symposium on Electron and Photon Interactions at High Energy (Daresbury Nuclear Physics Laboratory, Daresbury, England, 1969); S. J. Brodsky and S. D. Drell, Ann. Rev. Nucl. Sci. 20, 147 (1970).
12. K. W. Rothe and A. M. Wolsky, Nucl. Phys. B10, 241 (1969).
13. A. Barna et al., Phys. Rev. 173, 1391 (1968).

14. V. Alles-Borelli et al., Letters Nuovo Cimento 4, 1156 (1970);
A. K. Mann, Letters Nuovo Cimento 1, 486 (1971);
J. J. Sakurai, Letters Nuovo Cimento 1, 624 (1971);
E. W. Beier, Letters Nuovo Cimento 1, 1118 (1971).

15. R. Hofstadter, Ann. Rev. Nucl. Sci. 7, 231 (1957).

16. J. G. Rutherglen in Proceedings of the 4th International Symposium on Electron and Photon Interactions at High Energy (Daresbury Nuclear Physics Laboratory, Daresbury, England, 1969).

17. K. J. Barnes, Nuovo Cimento 27, 228 (1963).

18. S. D. Drell, Ann. Phys. 4, 75 (1958).

19. B. DeTollis, Nuovo Cimento 16, 203 (1960).

20. J. A. McClure and S. D. Drell, Nuovo Cimento 37, 1638 (1965).

21. I. Yu. Kobzarev and L. B. Okun, Soviet Physics JETP 14, 859 (1962).

22. D. Kiang and S. H. Ng, Phys. Rev. D2, 1964 (1970) and references contained therein.

23. J. Bernstein et al., Phys. Rev. 132, 1227 (1963).

24. E. Picasso in High Energy Physics and Nuclear Structure, 1970 (Plenum Press, New York, 1970); J. Bailey et al., Nuovo Cimento, to be published.

25. J. C. Wesley and A. Rich, Phys. Rev. Letters 24, 1320 (1970).

26. S. Rock et al., Phys. Rev. Letters 24, 748 (1970).

27. R. von Gehlen, Phys. Rev. 118, 1455 (1960).

28. S. D. Drell and J. D. Walecka, Ann. Phys. (N.Y.) 28, 18 (1964).

29. L. N. Hand, Phys. Rev. 129, 1834 (1963).

30. Muons from μ-e scatterings have too small a scattering angle (maximum ~5 mrad) to cause triggers in our system, and hence give no background.

31. J. Schwinger, Phys. Rev. 76, 760 (1949).

32. Y. S. Tsai in Proceedings of the Nucleon Structure Conference at Stanford, 1963 (Stanford University Press, Stanford, California, 1964).

33. L. W. Mo and Y. S. Tsai, Rev. Mod. Phys. 41, 205 (1969).

34. A. S. Dufner and Y. S. Tsai, Phys. Rev. 168, 1801 (1968).

35. H. L. Lynch et al., Phys. Rev. 164, 1635 (1967).

36. F. W. Brasse et al., DESY Report No. 67/34 (1967).

37. E. D. Bloom et al., Phys. Rev. Letters 23, 930 (1969);
M. Breidenbach et al., Phys. Rev. Letters 23, 935 (1969);
R. E. Taylor in Proceedings of the 4th International Symposium on Electron and Photon Interactions at High Energy (Daresbury Nuclear Physics Laboratory, Daresbury, England, 1969).

38. J. D. Bjorken and E. A. Paschos, Phys. Rev. 185, 1975 (1969);
for a general review see F. J. Gilman in Proceedings of the 4th International Symposium on Electron and Photon Interactions at High Energy (Daresbury Nuclear Physics Laboratory, Daresbury, England, 1969).

39. As shown in Ref. 37 of this paper, little change is produced in νW_2 if a relatively larger value is picked σ_S, for example if $\sigma_S/\sigma_T = 1$. Very little is known about the ratio σ_S/σ_T for $|q^2| < 1$ (GeV/c)^2. For higher values of $|q^2|$ as shown in Ref. 37, σ_S/σ_T is less than 0.3.

40. D. O. Caldwell et al., Phys. Rev. Letters 25, 609 (1970).

41. J. Ballam et al., Phys. Rev. Letters 23, 498 (1969) and J. Ballam et al., Phys. Rev. Letters 21, 1544 (1968).

42. H. Meyer et al., Phys. Letters 33B, 189 (1970).

43. V. Alles Borelli et al., paper submitted to the Amsterdam International Conference on Elementary Particles, Amsterdam, June 30 - June 6, 1971, revised version submitted to Nuovo Cimento.

44. J. Perez-y-Jorba in Proceedings of the 4th International Symposium on Electron and Photon Interactions at High Energy (Daresbury Nuclear Physics Laboratory, Daresbury, England, 1969); J. E. Augustin et al., Laboratoire de L'Accelerateur Lineaire Report LAL 1221 (1969).

45. G. Barbiellini et al., Laboratori Nazionali di Frascati Report LNF-70/38 (1970).

46. W. C. Barber et al., Phys. Rev. D3, 2796 (1971).

LIST OF TABLES

TABLE I

Summary of the properties of the muon and electron

Property	Comparison between muon and electron	If property is different	
		Muon	Electron
Intrinsic spin	both 1/2		
Statistics	both Fermi-Dirac		
Fundamental equation	both Dirac equation		
Structure	both point particles (within present experimental precision as discussed in this article)		
Interact through the strong interactions	both no (within present experimental precision as discussed in the article)		
Interact through the electromagnetic interaction	both yes		
Magnitude of electric charge	same for both		
Sign of electric charge	both + or -, neither 0		
Gyromagnetic ratio	both given by quantum electrodynamics and particle's mass		
Interact through the weak interactions	both yes		
Magnitude of weak interaction coupling constant	same for both		
Associated neutrino	yes but different neutrinos	ν_μ	ν_e
Mass (MeV/c^2)		106	0.51

TABLE II

Position	Distance from Target	Horizontal Plane		Vertical Plane
		Magnification	Dispersion	Magnification
S1: Momentum Slit	30 meters	1.08	3.25 cm/%	4.1
S2: Second Focus	65 meters	0.93	.45 cm/%	3.7
F3: Third Focus	88 meters	0.72	.35 cm/%	3.4

TABLE III

Chamber Number	X (cm)	Height (cm)	Width (cm)	Number of Gaps
1	383.5	71.1	42.2	8
2	470.0	86.4	49.5	8
3	796.8	193.0	76.2	8
4	890.8	204.5	88.9	4
5	992.6	204.5	106.7	6
6	1039.6	204.5	106.7	6
7	1086.6	204.5	106.7	6
8	1134.9	204.5	106.7	6

TABLE IV

Quantity	Limits
X^2_{fiducial}	100
$\lvert\phi_y\rvert$	3.5 mrad
$\lvert\phi_z\rvert$	10.0 mrad
Magnification	$.0138 \leq M \leq .0140$

TABLE V

K GeV	$\|q^2\|$ $(GeV/c)^2$	Number of Events Full	Empty	$d^2\sigma_\mu/dq^2dK$ $nb/(GeV^3/c^2)$	$\sigma_{exp,\mu}$ μb	x	νW_2	Δ RAD %	ε
	.3 - .4	494	3	483. ± 27.	140.1 ± 7.7	.151	.302 ± .017	2.7	.933
	.4 - .6	1371	8	204. ± 6.4	100.3 ± 3.2	.202	.277 ± .009	2.3	.991
.6	.6 - .8	589	0	93.6 ± 4.0	82.1 ± 3.5	.262	.281 ± .012	1.4	.989
to	.8 - 1.2	445	2	39.6 ± 2.1	64.0 ± 3.4	.337	.270 ± .014	.5	.986
1.5	1.2 - 1.6	131	2	13.6 ± 1.6	42.0 ± 4.8	.415	.213 ± .025	- .3	.981
	1.6 - 2.0	49	1	5.8 ± 1.1	29.3 ± 5.5	.477	.169 ± .032	- .7	.976
	2.0 - 3.0	36	0	2.2 ± .38	19.1 ± 3.2	.559	.130 ± .022	- 1.5	.965
	3.0 - 4.0	2	0	.17 ± .13	4.0 ± 2.9	.640	.031 ± .023	- .7	.947
	.3 - .4	247	1	192. ± 14.2	84.1 ± 6.2	.085	.233 ± .016	4.3	.978
	.4 - .6	855	6	109. ± 4.4	76.6 ± 3.1	.118	.273 ± .011	3.3	.976
1.5	.6 - .8	388	3	53.4 ± 3.2	60.9 ± 3.6	.157	.284 ± .017	2.5	.973
to	.8 - 1.2	312	5	24.1 ± 1.9	46.2 ± 3.6	.210	.280 ± .022	1.8	.968
2.5	1.2 - 1.6	129	1	13.0 ± 1.3	43.1 ± 4.2	.272	.329 ± .032	.9	.961
	1.6 - 2.0	37	1	4.0 ± .9	21.0 ± 4.7	.324	.187 ± .042	.8	.953
	2.0 - 3.0	21	0	1.4 ± .32	13.2 ± 3.1	.400	.143 ± .033	.4	.937
	3.0 - 4.0	13	0	1.1 ± .31	20.1 ± 5.7	.483	.259 ± .073	- .5	.912
	.3 - .4	145	1	98.7 ± 10.3	66.0 ± 6.9	.059	.186 ± .019	6.1	.952
	.4 - .6	537	6	66.9 ± 3.6	69.2 ± 3.7	.082	.268 ± .014	4.6	.949
2.5	.6 - .8	238	1	33.8 ± 2.6	52.2 ± 4.0	.111	.271 ± .021	3.9	.944
to	.8 - 1.2	213	0	18.7 ± 1.4	46.2 ± 3.4	.151	.320 ± .023	3.0	.937
3.5	1.2 - 1.6	76	1	7.8 ± 1.1	31.2 ± 4.5	.199	.281 ± .040	2.5	.926
	1.6 - 2.0	43	0	5.9 ± .9	35.4 ± 5.6	.242	.381 ± .060	1.6	.915
	2.0 - 3.0	29	0	2.0 ± .4	21.0 ± 4.1	.308	.281 ± .055	1.6	.894
	3.0 - 4.0	4	1	.036 ± .78	.37 ± 8.0	.383	.006 ± .131	- 6.9	.860
	.25 - .4	399	2	121. ± 7.5	98.4 ± 6.1	.039	.266 ± .016	6.0	.900
	.4 - .6	443	5	37.7 ± 2.2	55.9 ± 3.3	.059	.225 ± .013	6.5	.894
3.5	.6 - .8	230	3	22.4 ± 2.0	50.6 ± 4.4	.081	.276 ± .024	5.4	.887
to	.8 - 1.2	193	3	11.3 ± 1.2	38.8 ± 4.0	.111	.289 ± .030	4.8	.877
5.0	1.2 - 1.6	74	2	5.3 ± 1.1	28.5 ± 6.1	.149	.280 ± .060	4.2	.862
	1.6 - 2.0	35	0	3.6 ± .6	28.7 ± 5.1	.184	.344 ± .061	3.6	.846
	2.0 - 2.6	21	0	1.8 ± .4	20.1 ± 4.6	.224	.290 ± .067	3.4	.825
	2.6 - 3.4	13	0	1.0 ± .3	17.2 ± 5.0	.273	.297 ± .087	3.0	.794
	.1 - .2	427	10	125. ± 11.9	76.8 ± 7.3	.013	.098 ± .009	15.6	.790
	.2 - .4	936	4	48.6 ± 2.2	61.0 ± 2.7	.026	.152 ± .007	12.1	.782
5.0	.4 - .6	327	0	23.2 ± 1.5	52.5 ± 3.3	.043	.213 ± .013	9.4	.772
to	.6 - .8	170	1	14.6 ± 1.4	49.5 ± 4.7	.059	.275 ± .026	7.9	.762
7.0	.8 - 1.2	138	1	7.7 ± .8	39.1 ± 4.2	.082	.301 ± .032	7.3	.746
	1.2 - 1.6	55	3	3.1 ± .8	23.3 ± 6.4	.111	.241 ± .066	7.3	.723
	1.6 - 2.0	21	0	2.1 ± .5	22.5 ± 5.3	.138	.287 ± .068	6.5	.700
	.1 - .2	286	4	89. ± 9.4	81.3 ± 8.5	.010	.101 ± .011	21.5	.625
7.0	.2 - .4	412	4	29.9 ± 2.4	54.7 ± 4.3	.020	.134 ± .011	18.5	.615
to	.4 - .6	120	1	14.6 ± 1.8	46.4 ± 5.8	.034	.186 ± .023	14.4	.601
8.3	.6 - .8	61	0	10.6 ± 1.6	49.3 ± 7.4	.046	.272 ± .041	11.4	.567
	.8 - 1.0	30	1	5.6 ± 1.9	33.8 ± 11.6	.059	.236 ± .081	12.1	.573

1926C13

TABLE VI

K (GeV)	$\|q^2\|$ $(GeV/c)^2$	$\sigma_{exp,e}$ (μb)	K (GeV)	$\|q^2\|$ $(GeV/c)^2$	$\sigma_{exp,e}$ (μb)	K (GeV)	$\|q^2\|$ $(GeV/c)^2$	$\sigma_{exp,e}$ (μb)
	0.0	225. ± 13.5		0.0	146.8 ± 8.8		0.0	128.6 ± 7.7
	0.441	121. ± 0.7		0.302	78.9 ± 4.6		0.408	61.7 ± 5.1
.6	0.929	74.3 ± 0.5	2.5	0.740	56.7 ± 2.1	5.0	1.024	35.9 ± 1.8
to	1.141	60.8 ± 0.5	to	0.792	54.2 ± 3.0	to	1.391	29.6 ± 2.4
1.5	1.714	38.0 ± 0.3	3.5	1.473	37.8 ± 0.6	7.0	1.602	28.4 ± 1.0
	2.410	23.1 ± 0.2		2.116	25.7 ± 0.5		2.513	18.6 ± 1.0
	2.813	18.1 ± 0.3		2.297	24.1 ± 1.0		3.372	14.5 ± 0.6
	4.210	8.2 ± 0.7		3.593	13.9 ± 0.5			
				4.558	10.1 ± 0.4			
	0.0	168.0 ± 10.1		0.0	137.3 ± 8.2		0.0	124.3 ± 7.5
	0.369	92.5 ± 0.7		0.250	78.7 ± 7.0		0.749	42.4 ± 2.4
1.5	0.832	59.7 ± 1.1	3.5	0.588	59.1 ± 2.8	7.0	1.002	36.2 ± 5.1
to	0.960	54.8 ± 1.4	to	1.263	35.8 ± 1.1	to	1.280	28.3 ± 1.6
2.5	1.584	36.6 ± 0.8	5.0	1.881	26.1 ± 0.6	8.3	1.840	22.3 ± 1.9
	2.259	25.2 ± 0.3		1.881	25.5 ± 1.4		2.632	15.6 ± 0.8
	2.606	22.7 ± 2.7		3.099	16.8 ± 0.8			
	3.896	10.8 ± 0.5		4.015	12.5 ± 0.6			

TABLE VII

K (GeV)	$\|q^2\|$ $(GeV/c)^2$	$\rho(q^2, K, 12\ GeV/c)$	K GeV	$\|q^2\|$ $(GeV/c)^2$	$\rho(q^2, K, 12\ GeV/c)$	K (GeV)	$\|q^2\|$ $(GeV/c)^2$	$\rho(q^2, K, 12\ GeV/c)$
	.35	1.04 ± .09		.35	.89 ± .10		.35	.86 ± .12
	.50	.89 ± .07		.50	.95 ± .09		.50	1.02 ± .11
.6	.70	.89 ± .08	1.5	.70	.90 ± .10	2.5	.70	.89 ± .11
to	1.00	.92 ± .09	to	1.00	.86 ± .10	to	1.00	.95 ± .12
1.5	1.40	.86 ± .13	2.5	1.40	1.04 ± .14	3.5	1.40	.81 ± .14
	1.80	.82 ± .18		1.80	.65 ± .16		1.80	1.14 ± .21
	2.50	.88 ± .19		2.50	.60 ± .15		2.50	.96 ± .22
	3.50	.32 ± .24		3.50	1.49 ± .46		3.50	.03 ± .56
	.325	1.26 ± .11		.15	.82 ± .09		.15	.91 ± .11
	.50	.88 ± .08		.30	.82 ± .06		.30	.78 ± .08
3.5	.70	.96 ± .11	5.0	.50	.89 ± .08	7.0	.50	.86 ± .13
to	1.00	.93 ± .12	to	.70	1.02 ± .12	to	.70	1.12 ± .19
5.0	1.40	.88 ± .20	7.0	1.00	1.02 ± .14	8.3	.90	.91 ± .32
	1.80	1.08 ± .21		1.40	.78 ± .22			
	2.30	.92 ± .23		1.80	.88 ± .22			
	3.00	.99 ± .30						

LIST OF FIGURES

14. Diagrams involved in the radiative corrections.

15. νW_2 values for the data of Table V, plotted versus $x=|q^2|/(2M\nu)=1/\omega$. x must lie between 0 and 1.0. A different symbol is used for each K interval. The leftmost point (smallest x) of each K bin is at the lowest value of $|q^2|$ in that K bin.

16. Map of the K, q^2 kinematic plane showing the continuous bins for which muon-proton inelastic scattering data is presented and the locations of the electron-proton data to which it is compared. The 6^o and 10^o measurements of Ref. 37 form a closely spaced array of data points along the heavy line segments in the low K regions. At higher K the e-p data points are widely separated and are indicated by discrete dots.

17. For each K interval the upper plot gives the experimental values of $\sigma_{exp,\mu}(q^2,K,p_\mu)$ denoted by a solid circle, $\sigma_{exp,e}(q^2,K,p_\mu)$ denoted by an x and $\sigma_{\gamma p}(K)$ denoted by a triangle; p_μ=12 GeV/c. These quantities are defined in the text. $\sigma_{exp,e}(q^2,K,p_\mu)$ is extrapolated from the data of Ref. 37 as described in the text. For each K interval the lower plot gives the values of $\rho_{inelastic}(q^2,K)=\sigma_{exp,\mu}(q^2,K,p_\mu)/\sigma_{exp,e}(q^2,K,p_\mu)$. The errors of $\sigma_{\gamma p}$ were set at $\pm 6\%$. In most cases the errors in $\sigma_{exp,e}$ were too small to be displayed. The error bars represent only statistical errors.

18. Contour plots for the parameters N'^2 and $\Lambda_D'^{-2}$ obtained by fitting the experimental values of the ratio $\rho_{inelastic}(q^2,K,12\ GeV/c)$ to the equation $\rho_{inelastic}(q^2,K,12\ GeV/c) = N'^2/(1.0+|q^2|/\Lambda_D'^2)^2$. The inner elipse represents one standard deviation and the outer elipse represents two standard deviations in the fit. The $\pm 8\%$ systematic error is not included, its effect is to allow the N'^2 scale to be shifted up and down by an amount as large as 0.08.

19. The values of $\rho_{elastic}(q^2)$, as defined in the text, versus $|q^2|$ from Ref. 2.

20. One photon exchange diagram and the hypothetical neutral vector boson (X) exchange diagram showing the various coupling constants.

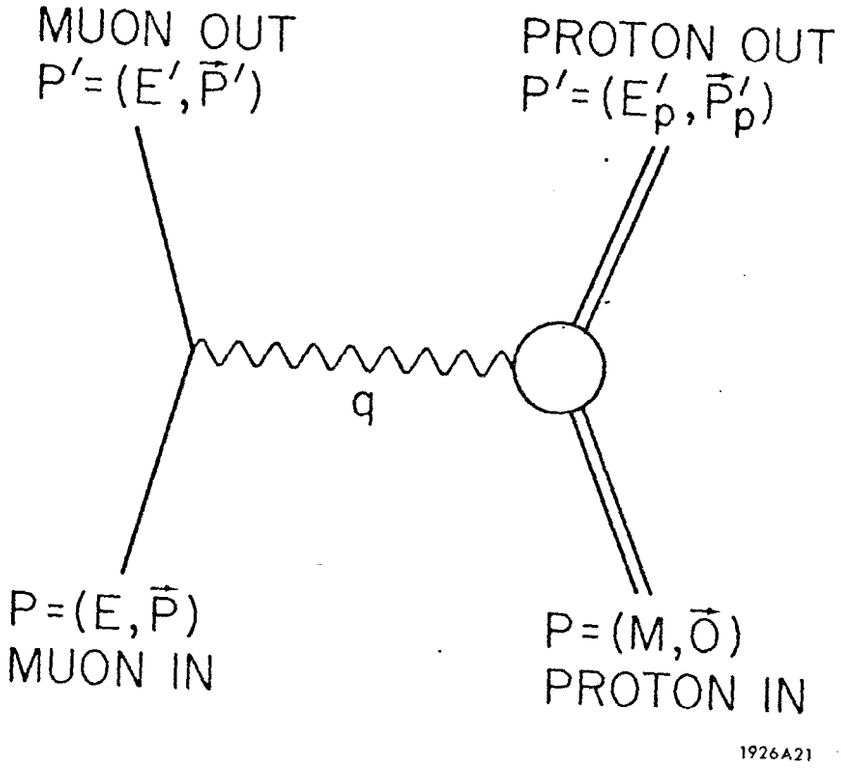
MUON OUT
P′=(E′,P⃗′)
PROTON OUT
P′=(E′p,P⃗′p)
q
P=(E,P⃗)
MUON IN
P=(M,O⃗)
PROTON IN
1926A21

Fig. 1

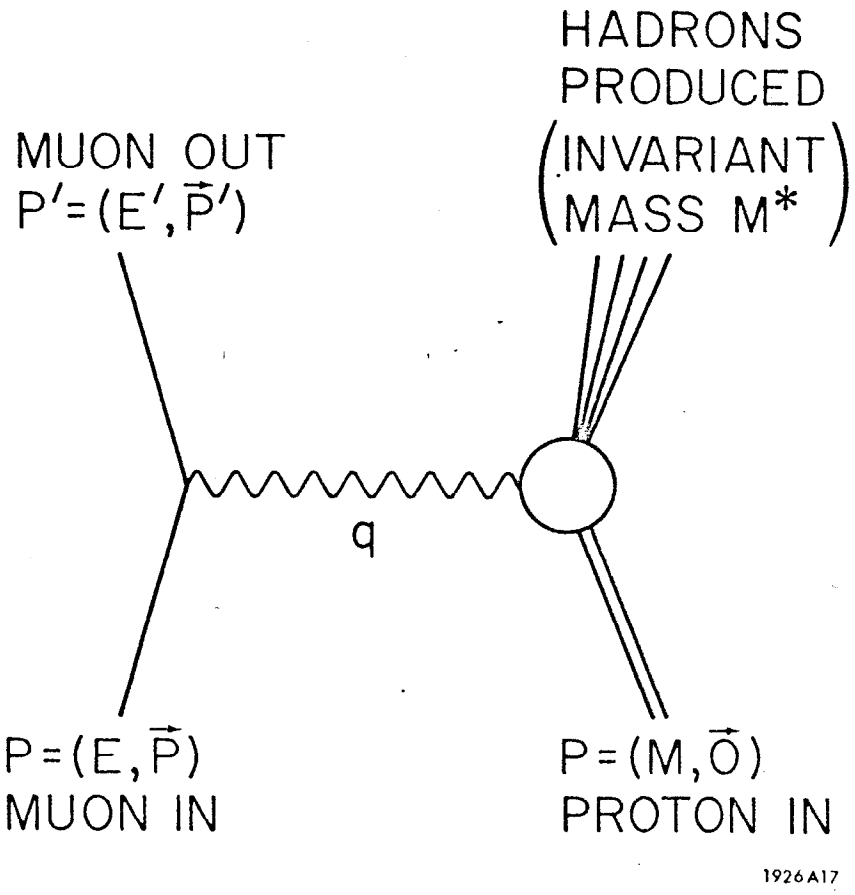
HADRONS
PRODUCED
(INVARIANT
MASS M*)
MUON OUT
P′=(E′,P⃗′)
q
P=(E,P⃗)
MUON IN
P=(M,O⃗)
PROTON IN
1926A17

Fig. 2

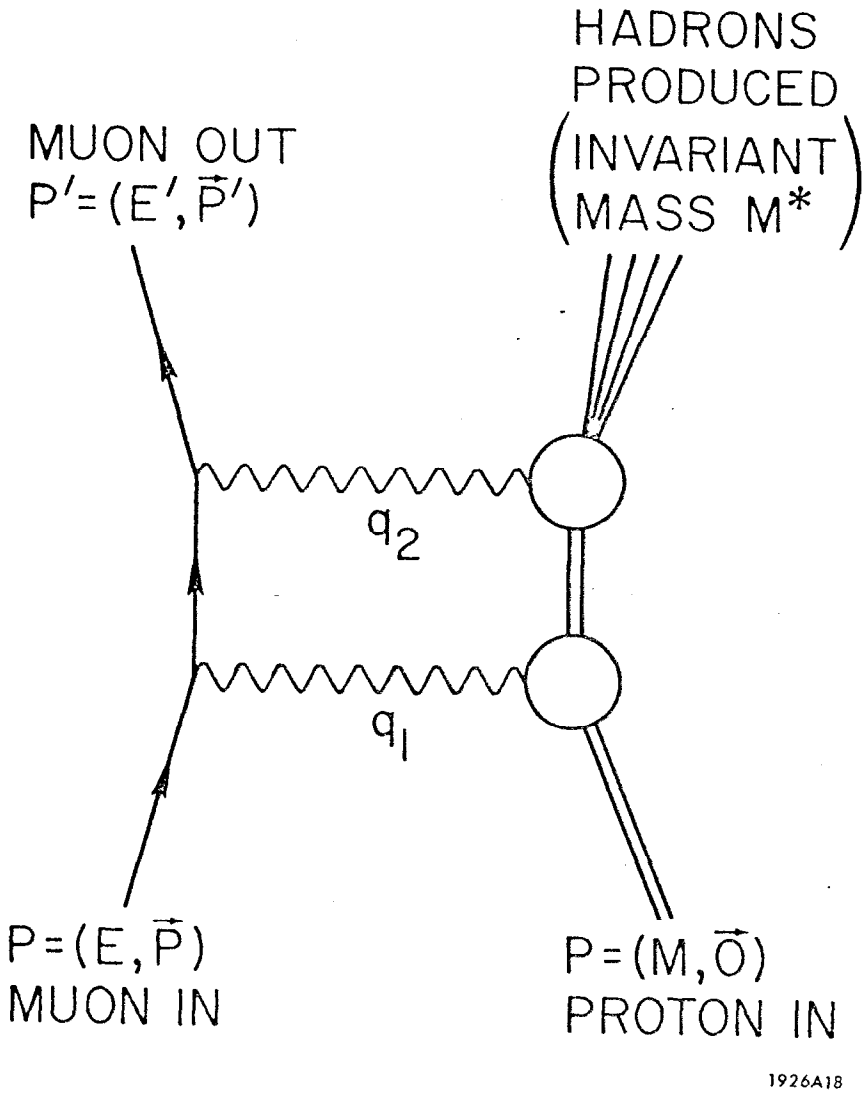
HADRONS
PRODUCED
(INVARIANT
MASS M*)
MUON OUT
P′=(E′,P⃗′)
q2
q1
P=(E,P⃗)
MUON IN
P=(M,O⃗)
PROTON IN
1926A18

Fig. 3

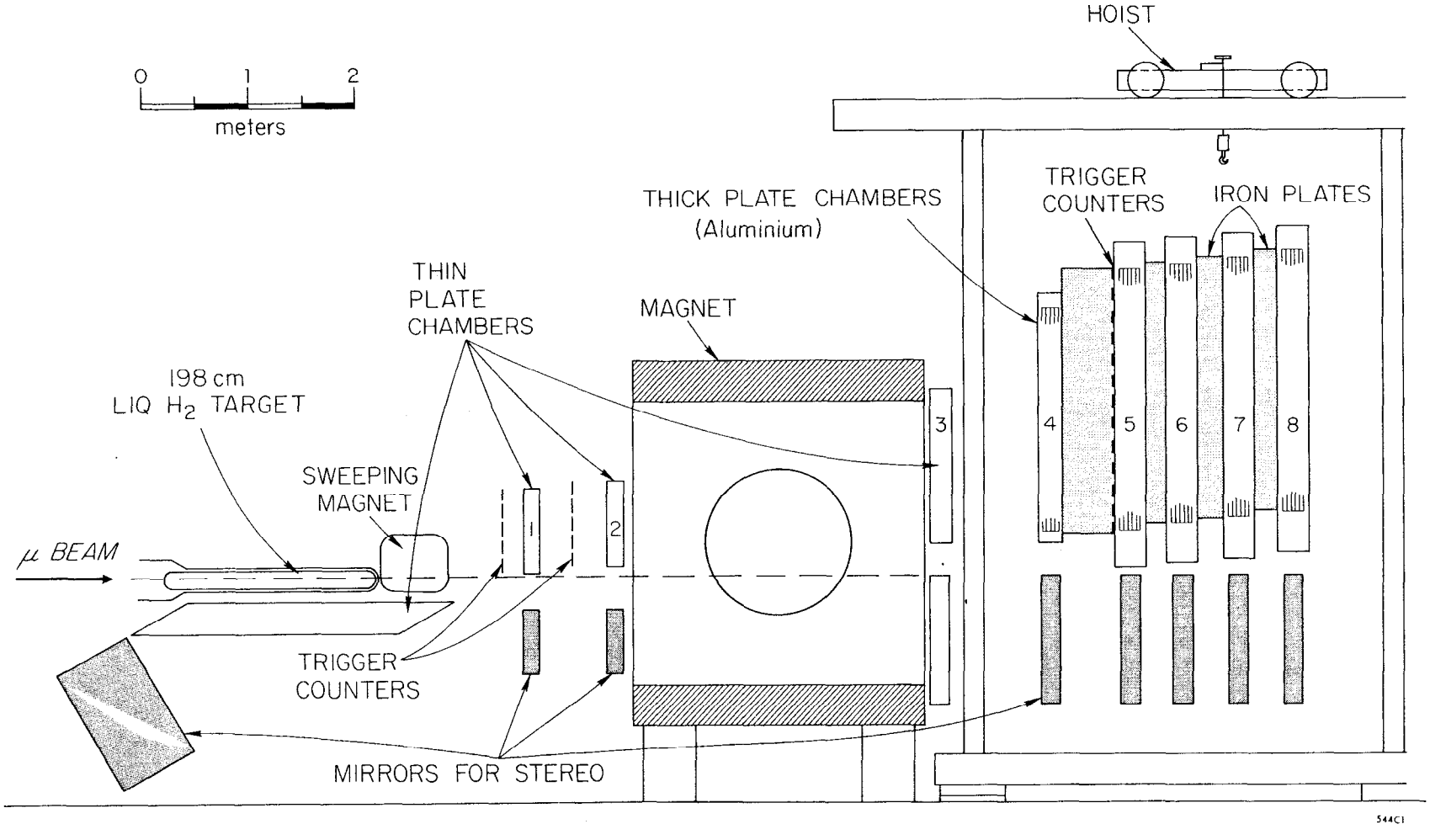
0
1
2
meters
HOIST
TRIGGER
COUNTERS
IRON PLATES
THICK PLATE CHAMBERS
(Aluminium)
THIN
PLATE
CHAMBERS
MAGNET
198 cm
LIQ H_2 TARGET
SWEEPING
MAGNET
μ BEAM
1
2
3
4
5
6
7
8
TRIGGER
COUNTERS
MIRRORS FOR STEREO
544C1

Fig. 4

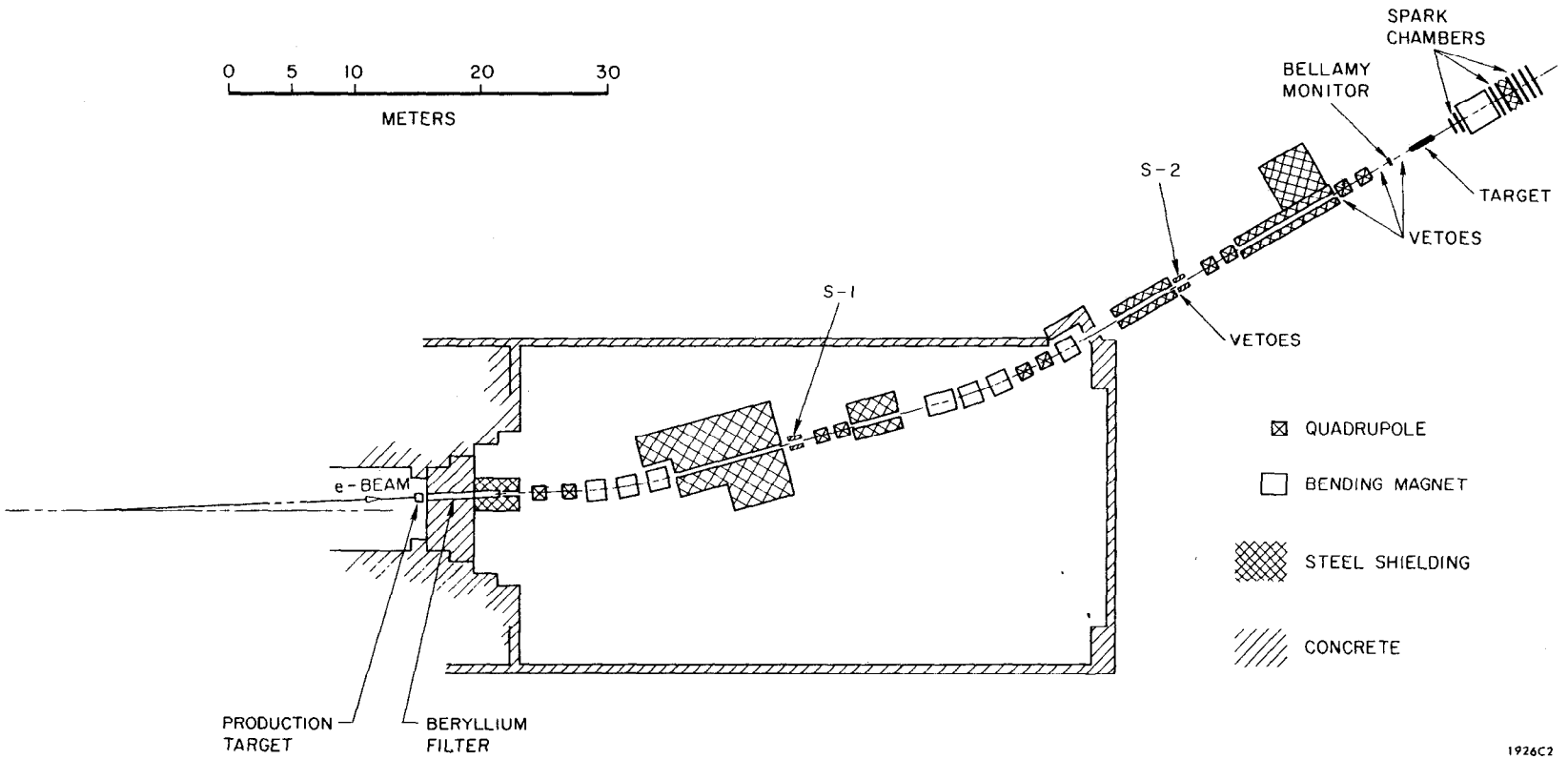
0 5 10 20 30
METERS
SPARK CHAMBERS
BELLAMY MONITOR
TARGET
VETOES
S-2
S-1
VETOES
e-BEAM
QUADRUPOLE
BENDING MAGNET
STEEL SHIELDING
CONCRETE
PRODUCTION TARGET
BERYLLIUM FILTER
1926C2

Fig. 5

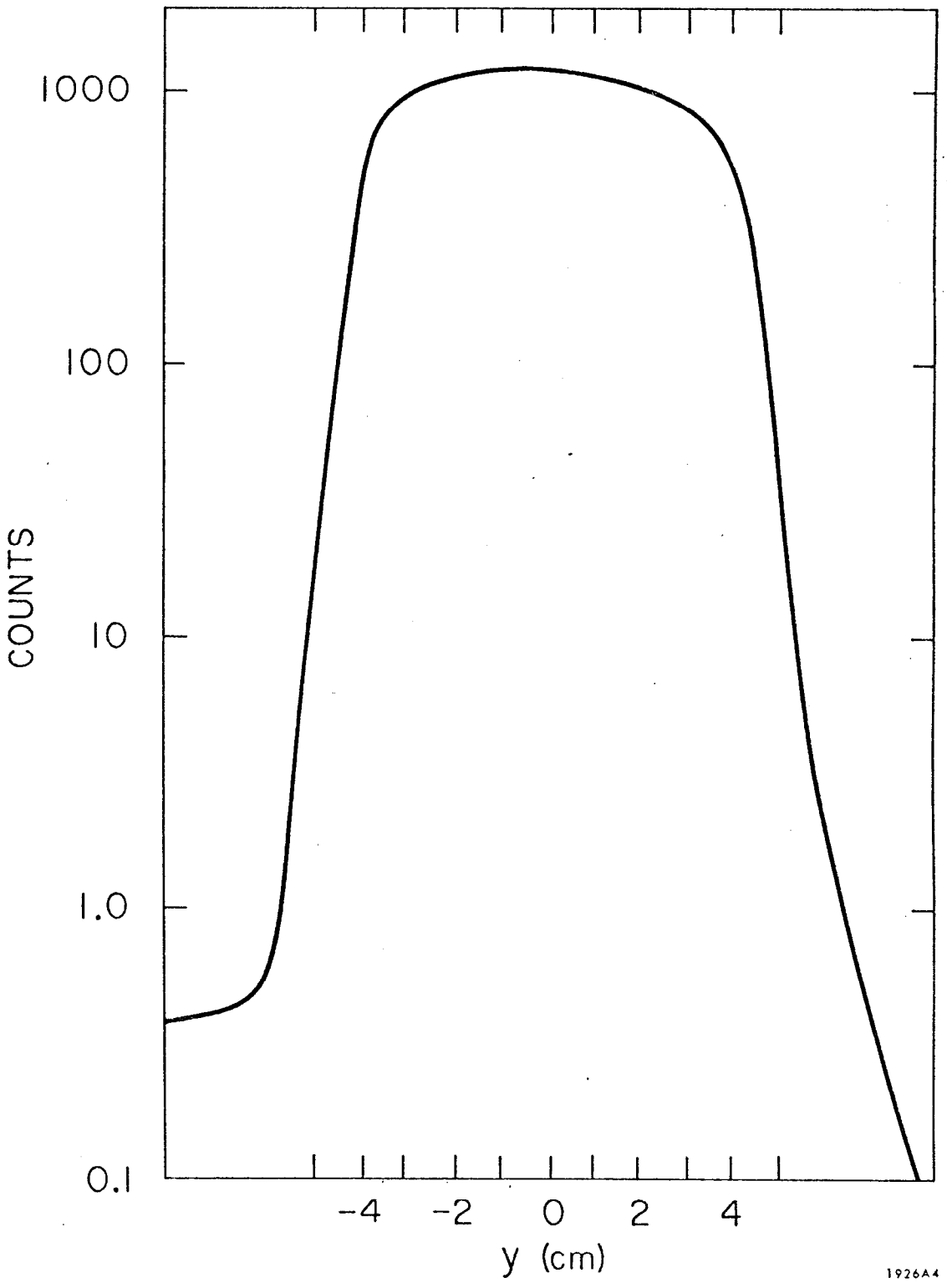

Fig. 6

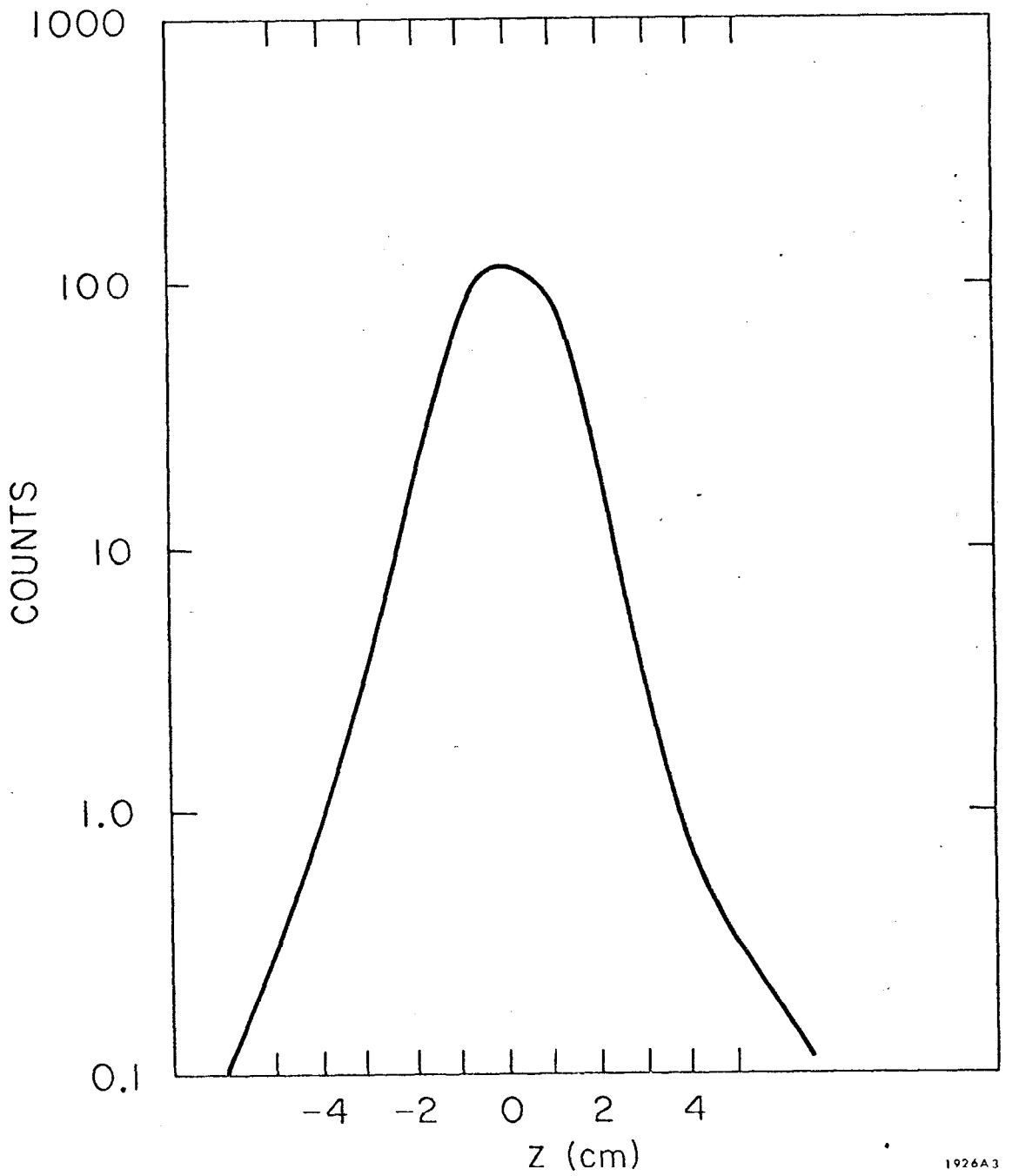

Fig 7

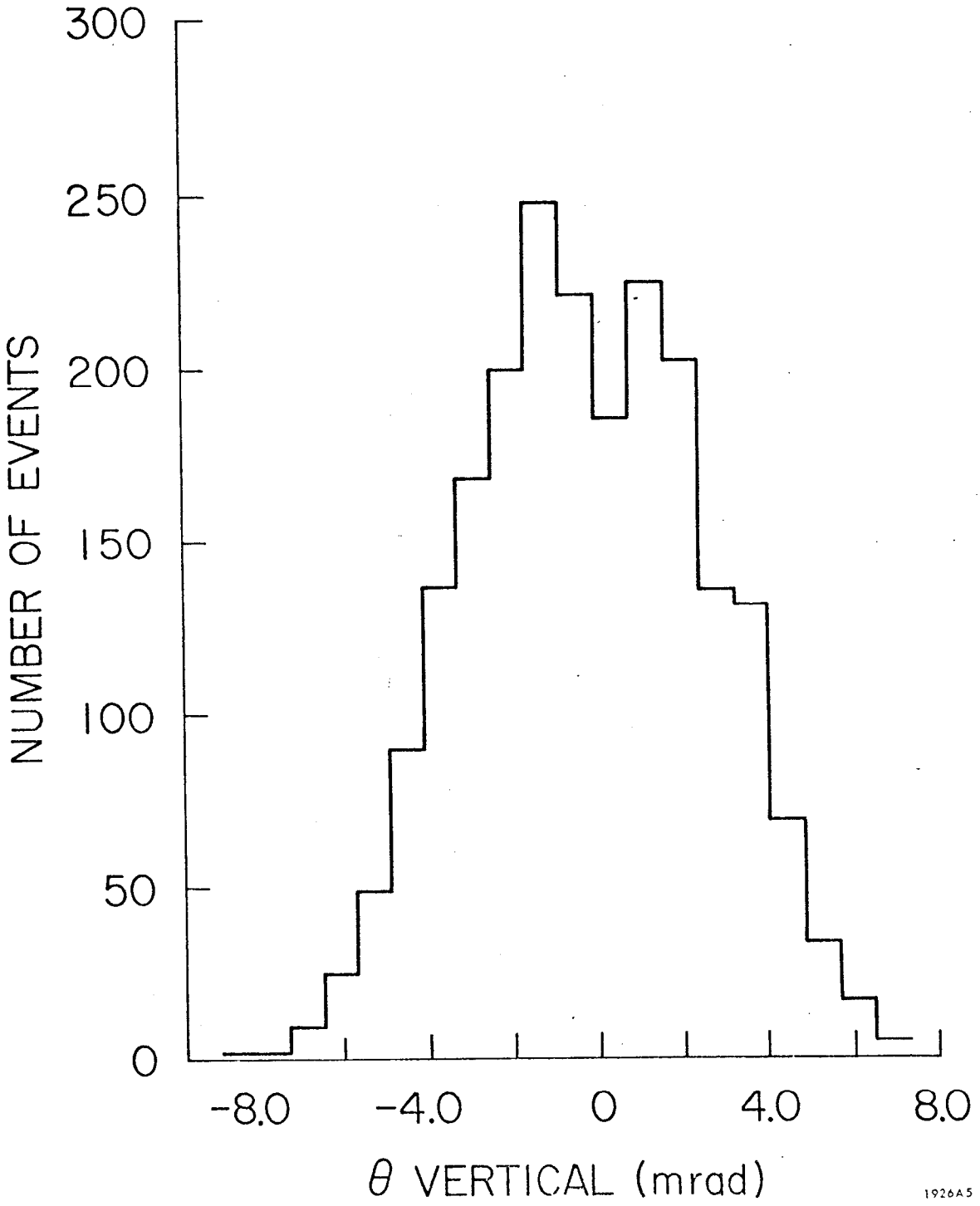
300
250
200
150
100
50
0
NUMBER OF EVENTS
-8.0
-4.0
0
4.0
8.0
θ VERTICAL (mrad)
1926A5

Fig. 8

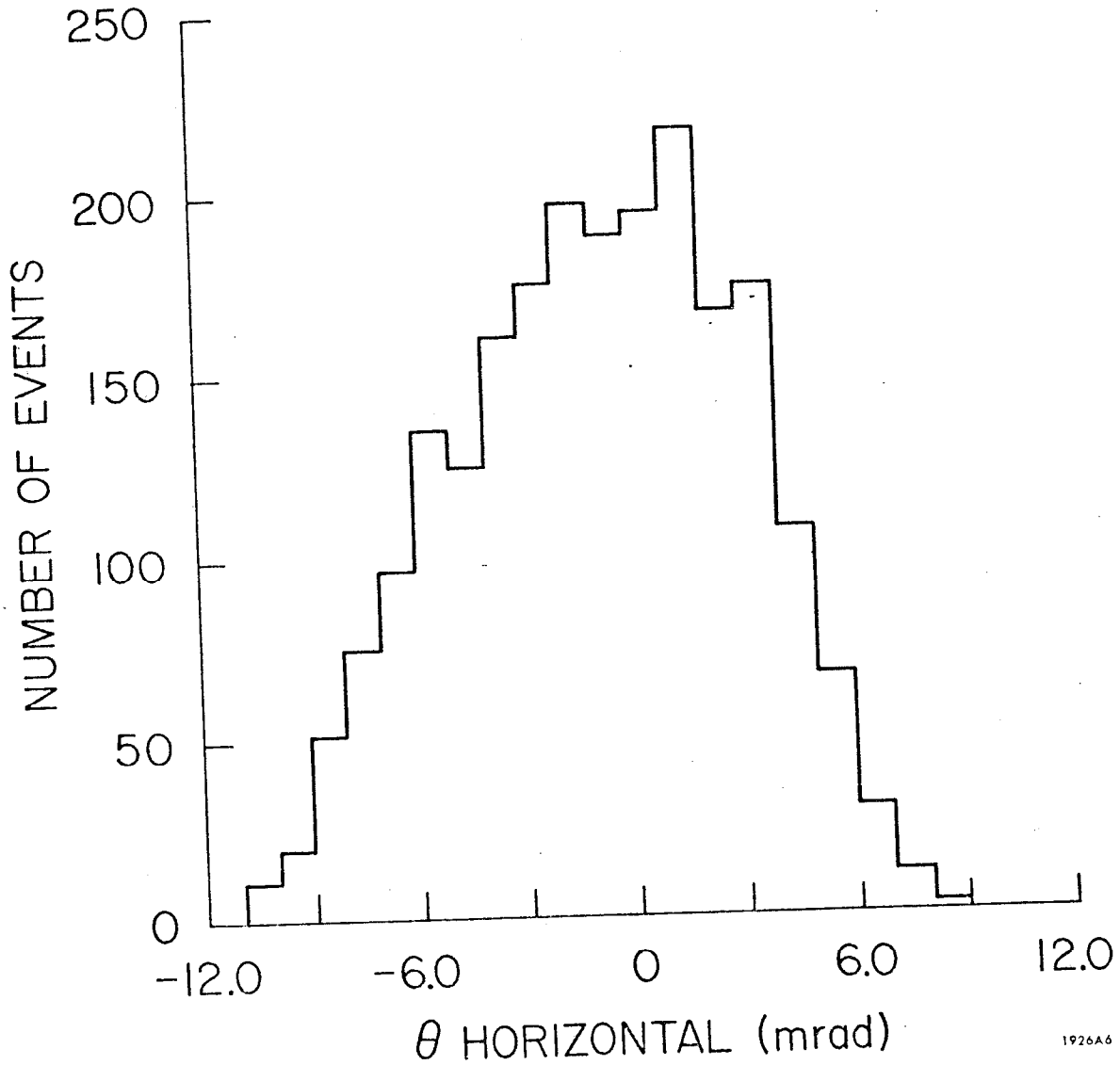
250
200
150
100
50
0
NUMBER OF EVENTS
-12.0
-6.0
0
6.0
12.0
θ HORIZONTAL (mrad)
1926A6

Fig. 9

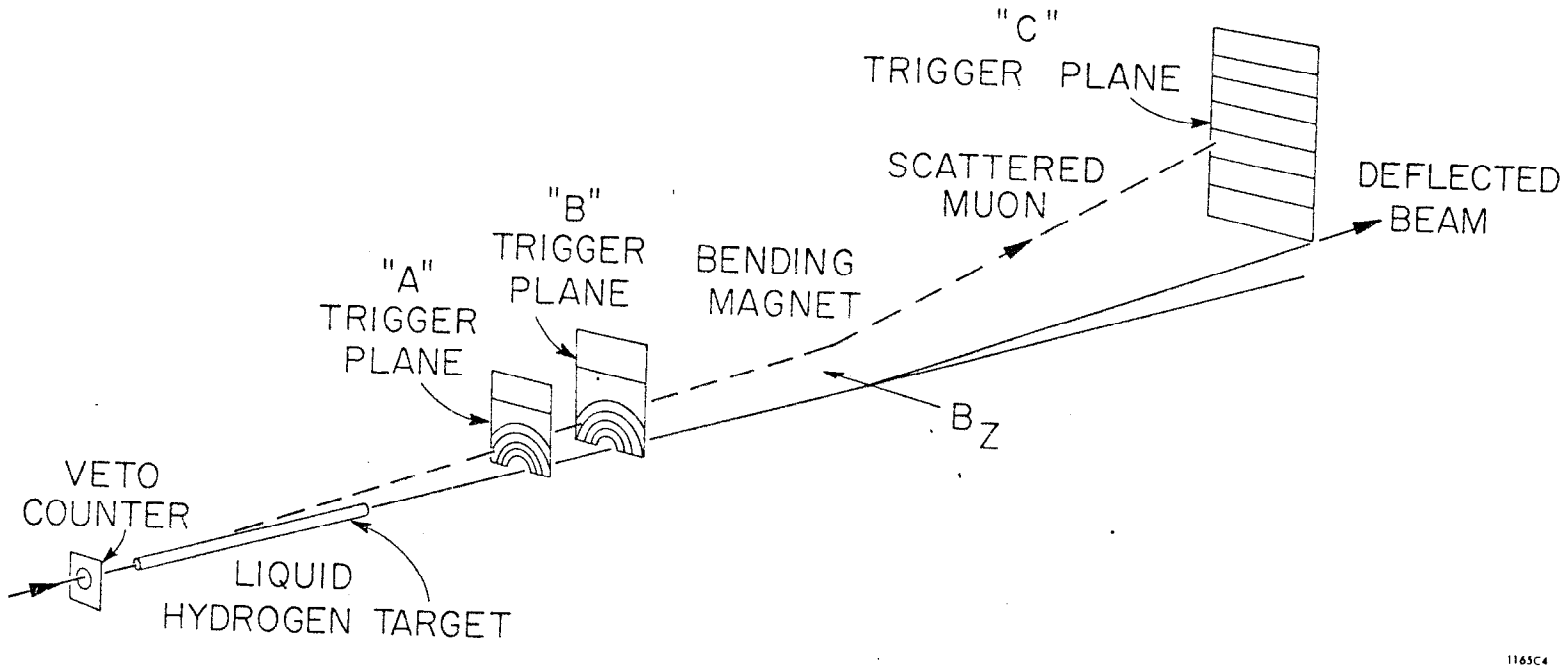
"C"
TRIGGER PLANE
SCATTERED
MUON
DEFLECTED
BEAM
"B"
TRIGGER
PLANE
"A"
TRIGGER
PLANE
BENDING
MAGNET
B_Z
VETO
COUNTER
LIQUID
HYDROGEN TARGET
1165C4

Fig. 10

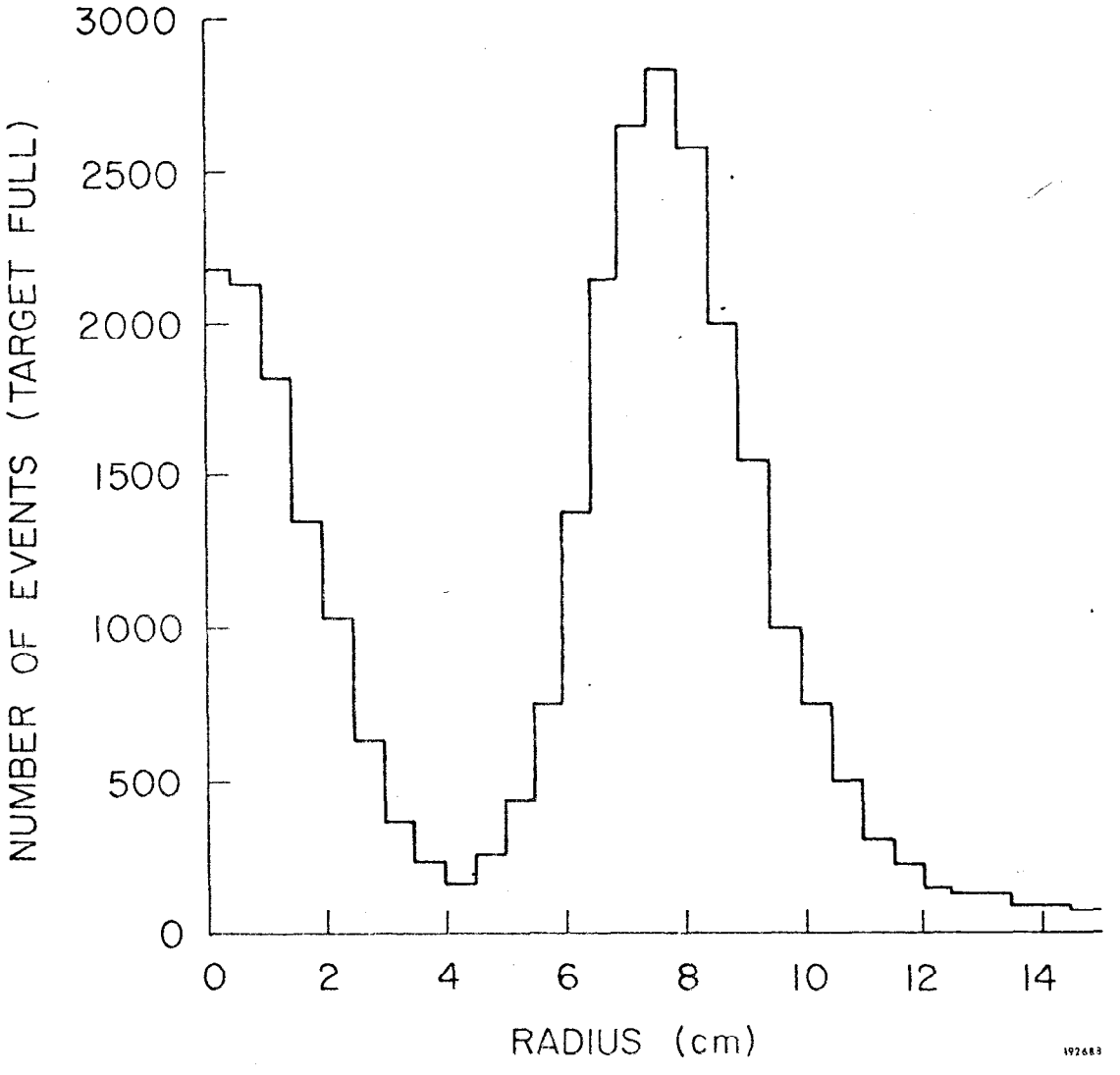
3000
2500
2000
1500
1000
500
0
NUMBER OF EVENTS (TARGET FULL)
0
2
4
6
8
10
12
14
RADIUS (cm)

Fig. 11a

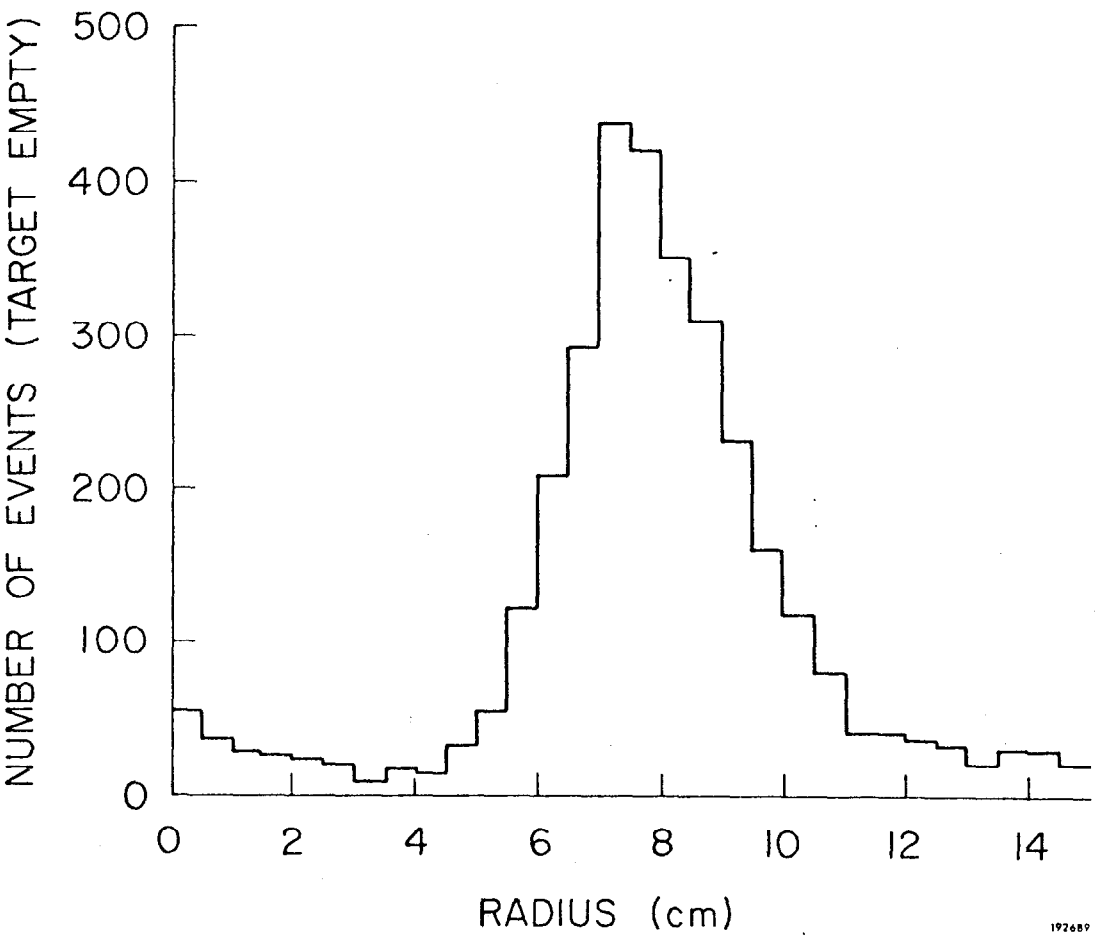
NUMBER OF EVENTS (TARGET EMPTY)
500
400
300
200
100
0
0
2
4
6
8
10
12
14
RADIUS (cm)
192689

Fig. 11b

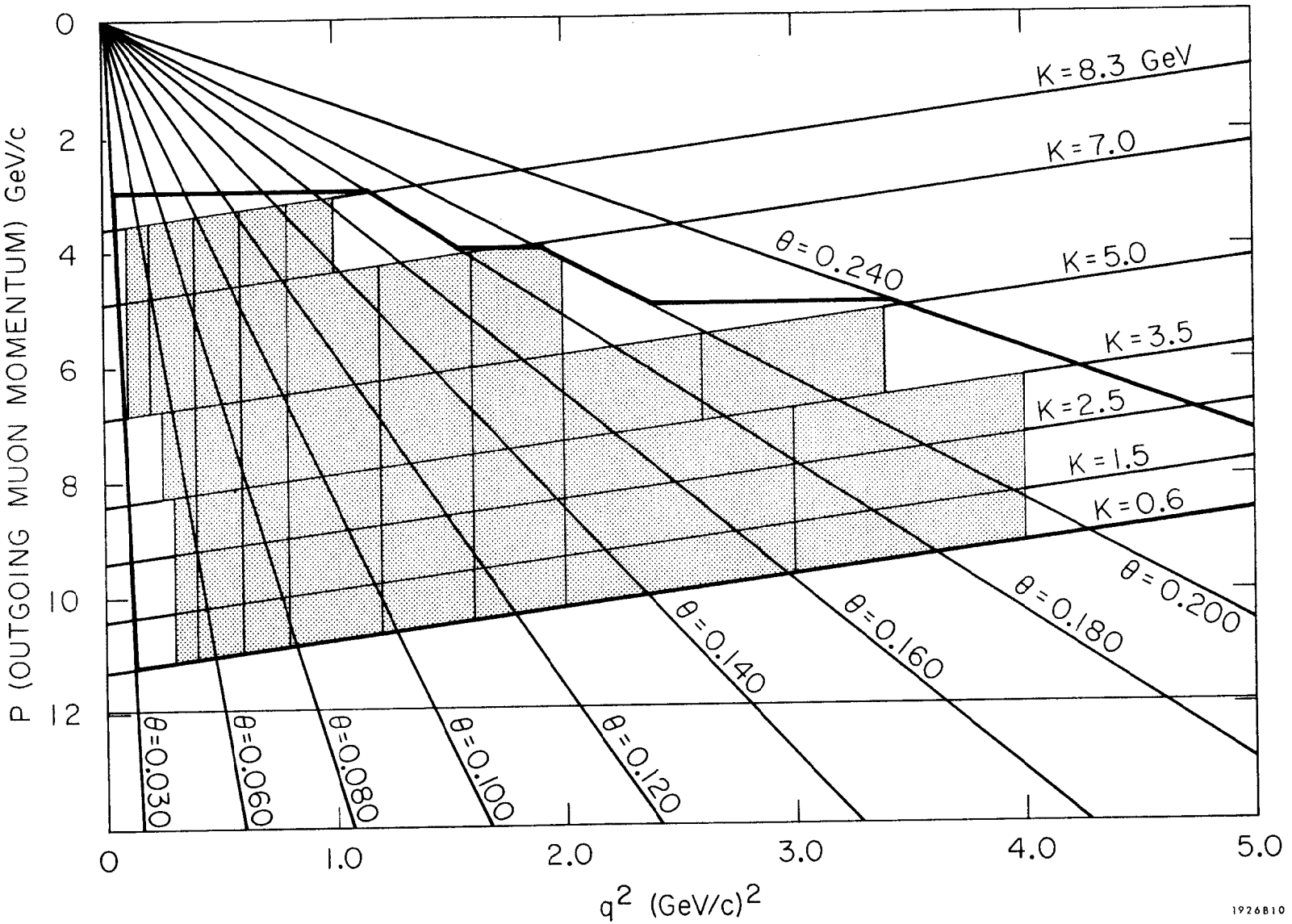
P (OUTGOING MUON MOMENTUM) GeV/c
0
2
4
6
8
10
12
K = 8.3 GeV
K = 7.0
K = 5.0
K = 3.5
K = 2.5
K = 1.5
K = 0.6
θ = 0.240
θ = 0.200
θ = 0.180
θ = 0.160
θ = 0.140
θ = 0.120
θ = 0.100
θ = 0.080
θ = 0.060
θ = 0.030
0
1.0
2.0
3.0
4.0
5.0
q² (GeV/c)²
1926B10

Fig. 12

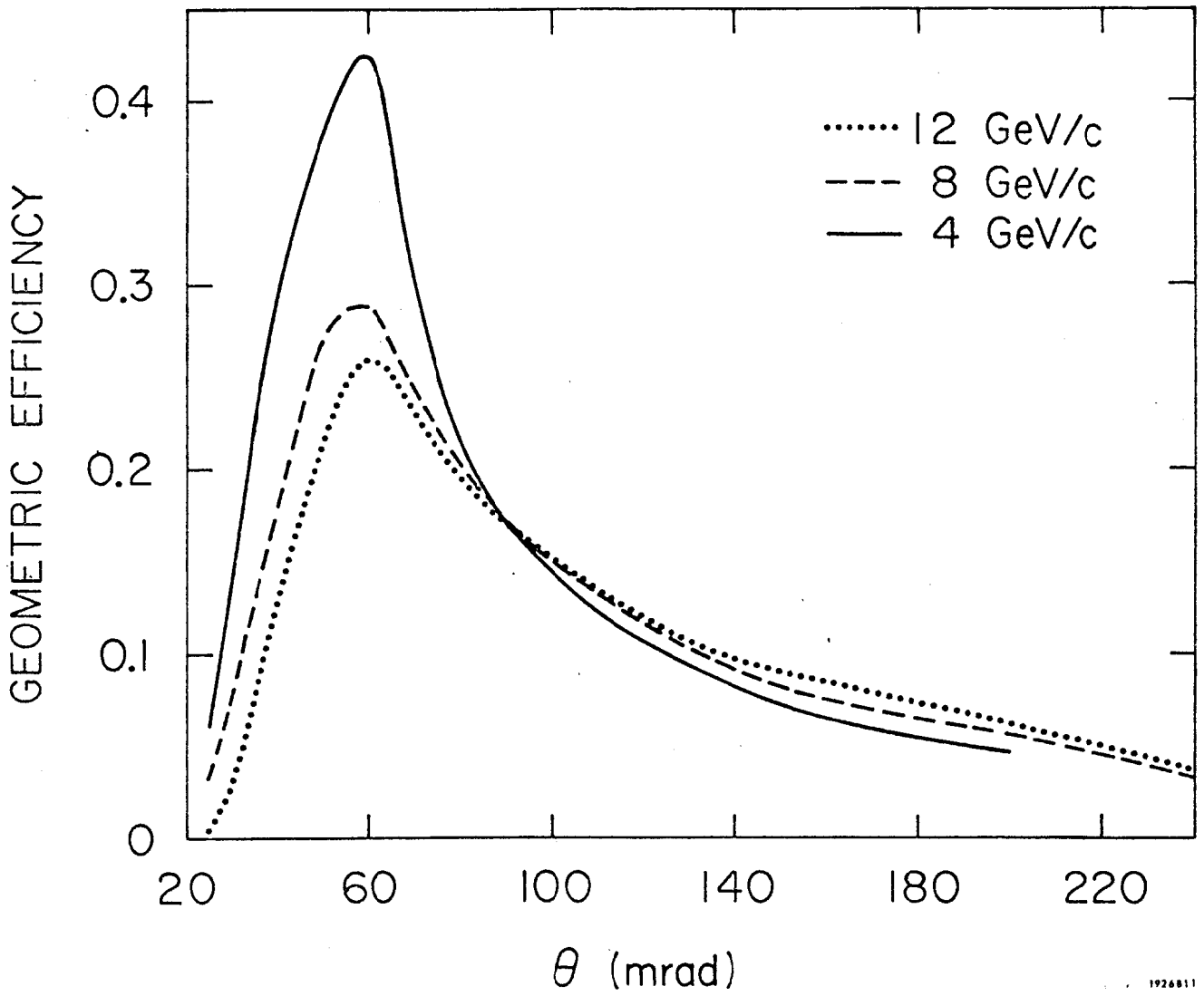
GEOMETRIC EFFICIENCY
0.4
0.3
0.2
0.1
0
20
60
100
140
180
220
θ (mrad)
12 GeV/c
8 GeV/c
4 GeV/c
1926B11

Fig. 13

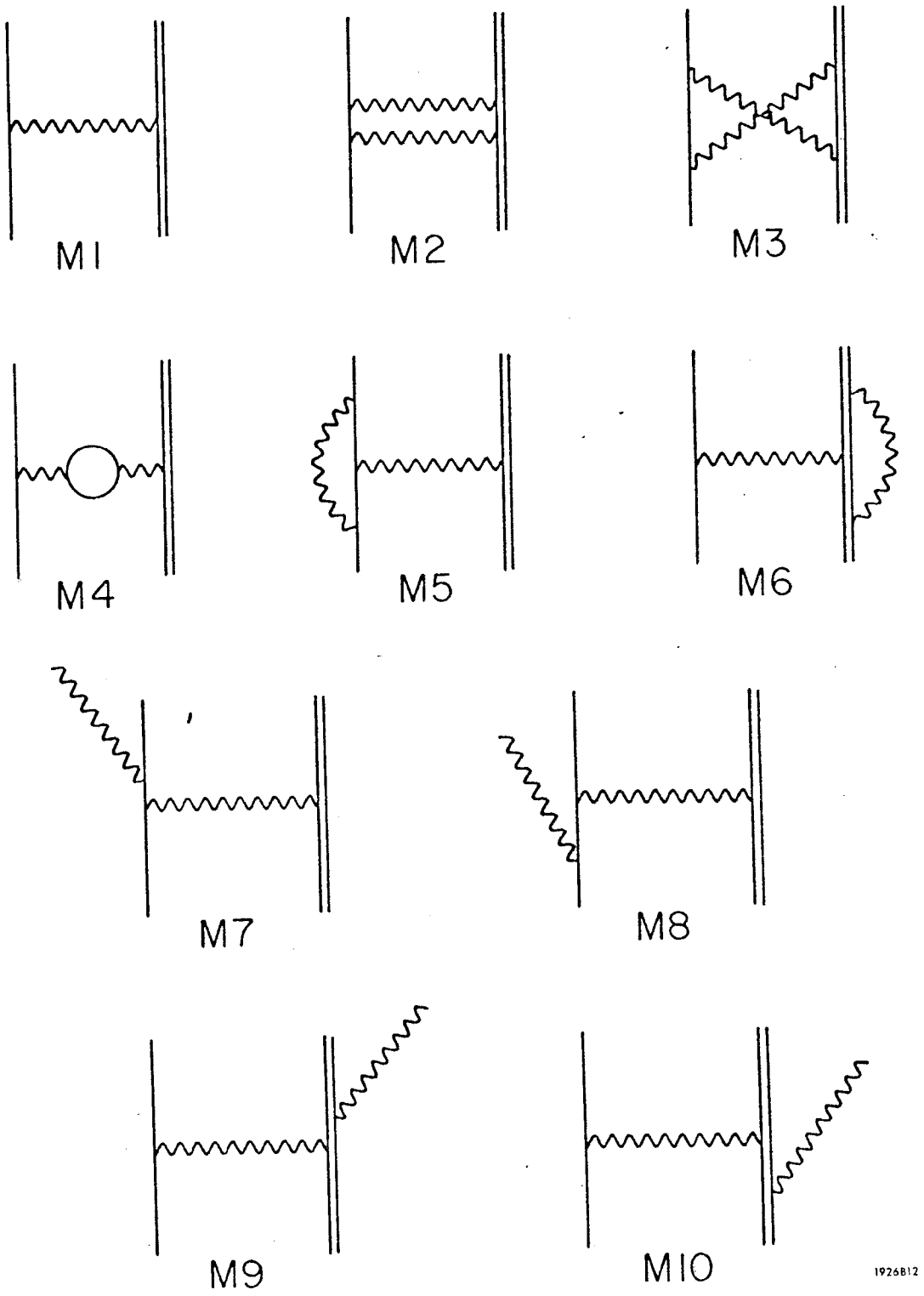

Fig. 14

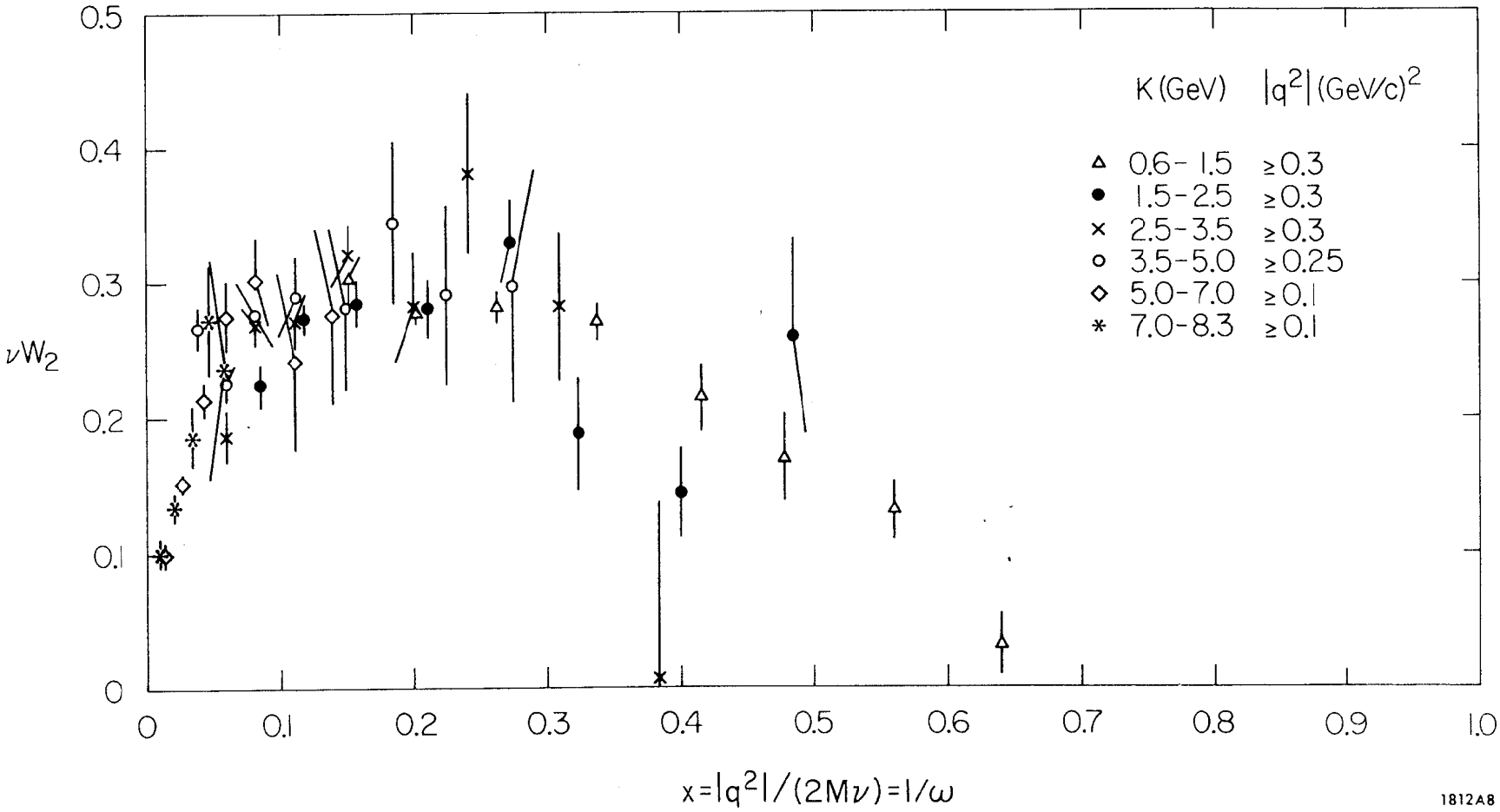
0.5
0.4
0.3
0.2
0.1
0
νW_2
0
0.1
0.2
0.3
0.4
0.5
0.6
0.7
0.8
0.9
1.0
$x = |q^2|/(2M\nu) = 1/\omega$
K (GeV) $|q^2|$ (GeV/c)^2
△ 0.6 - 1.5 ≥0.3
● 1.5-2.5 ≥0.3
× 2.5-3.5 ≥0.3
○ 3.5-5.0 ≥0.25
◇ 5.0-7.0 ≥0.1
* 7.0-8.3 ≥0.1
1812A8

Fig. 15

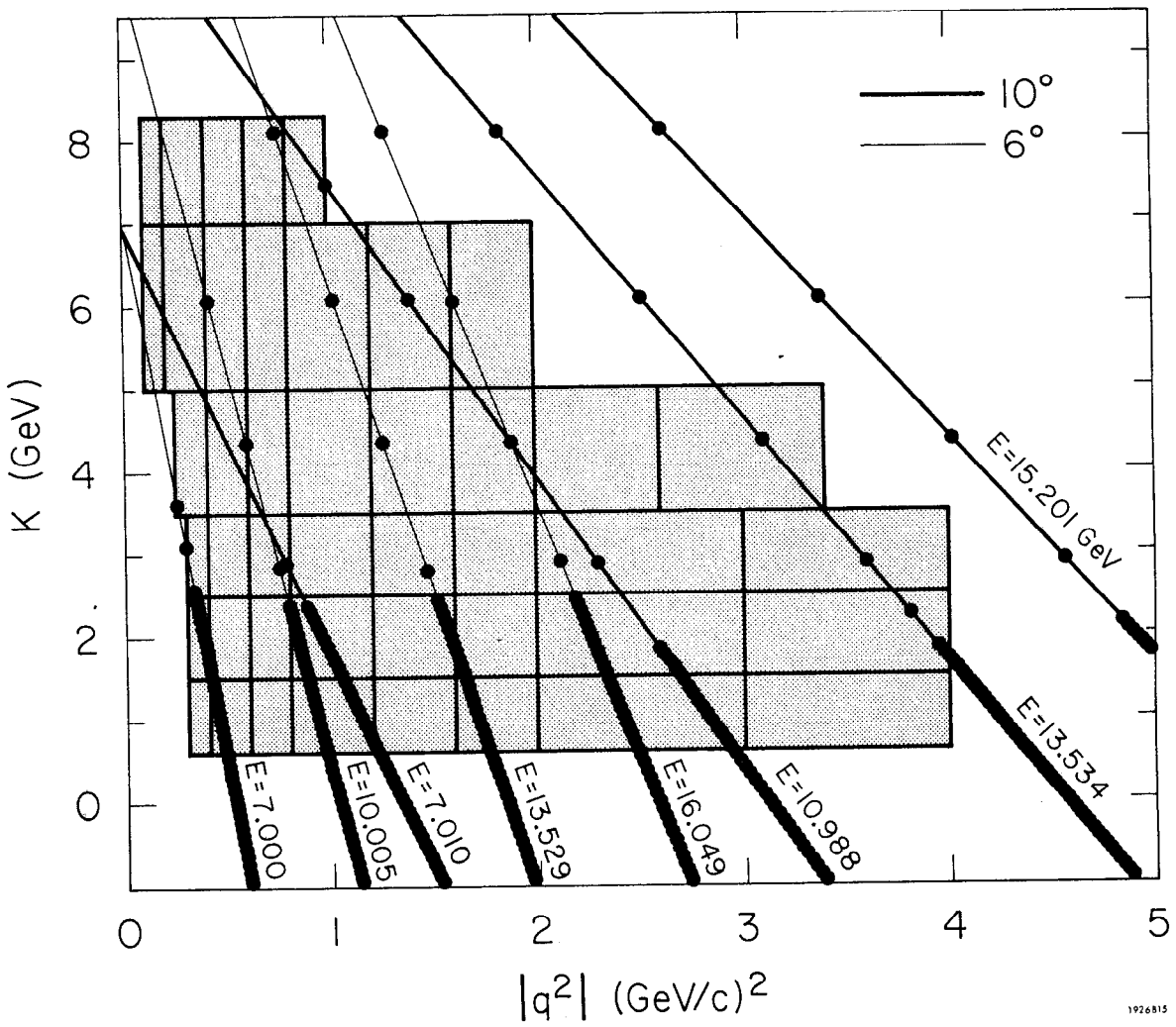
10°
6°
E=15.201 GeV
E=13.534
E=10.988
E=16.049
E=13.529
E=7.010
E=10.005
E=7.000
K (GeV)
0
2
4
6
8
0
1
2
3
4
5
|q²| (GeV/c)²
1926815

Fig. 16

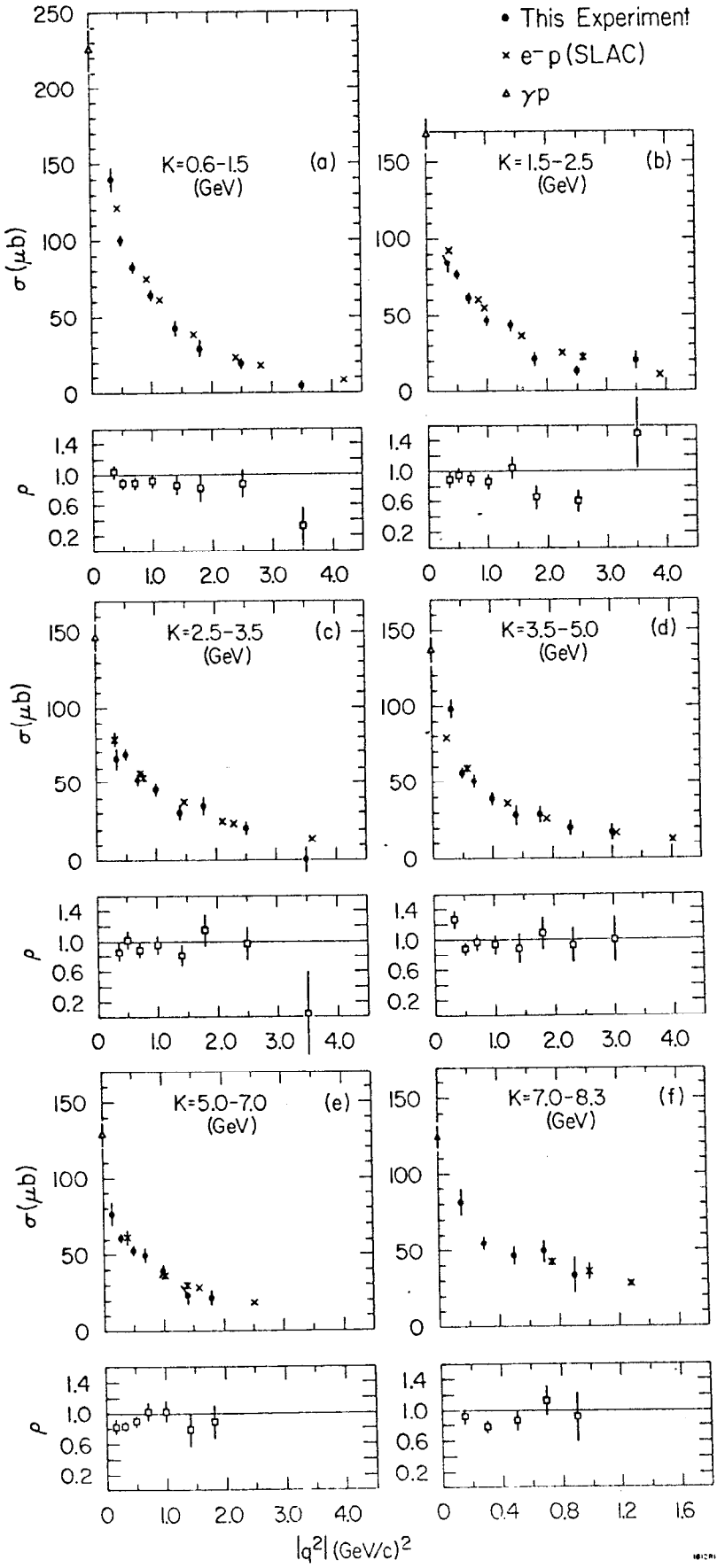
• This Experiment
× e⁻p (SLAC)
▲ γp
K=0.6-1.5 (GeV) (a)
K=1.5-2.5 (GeV) (b)
K=2.5-3.5 (GeV) (c)
K=3.5-5.0 (GeV) (d)
K=5.0-7.0 (GeV) (e)
K=7.0-8.3 (GeV) (f)
σ(μb)
ρ
|q²| (GeV/c)²

Fig. 17

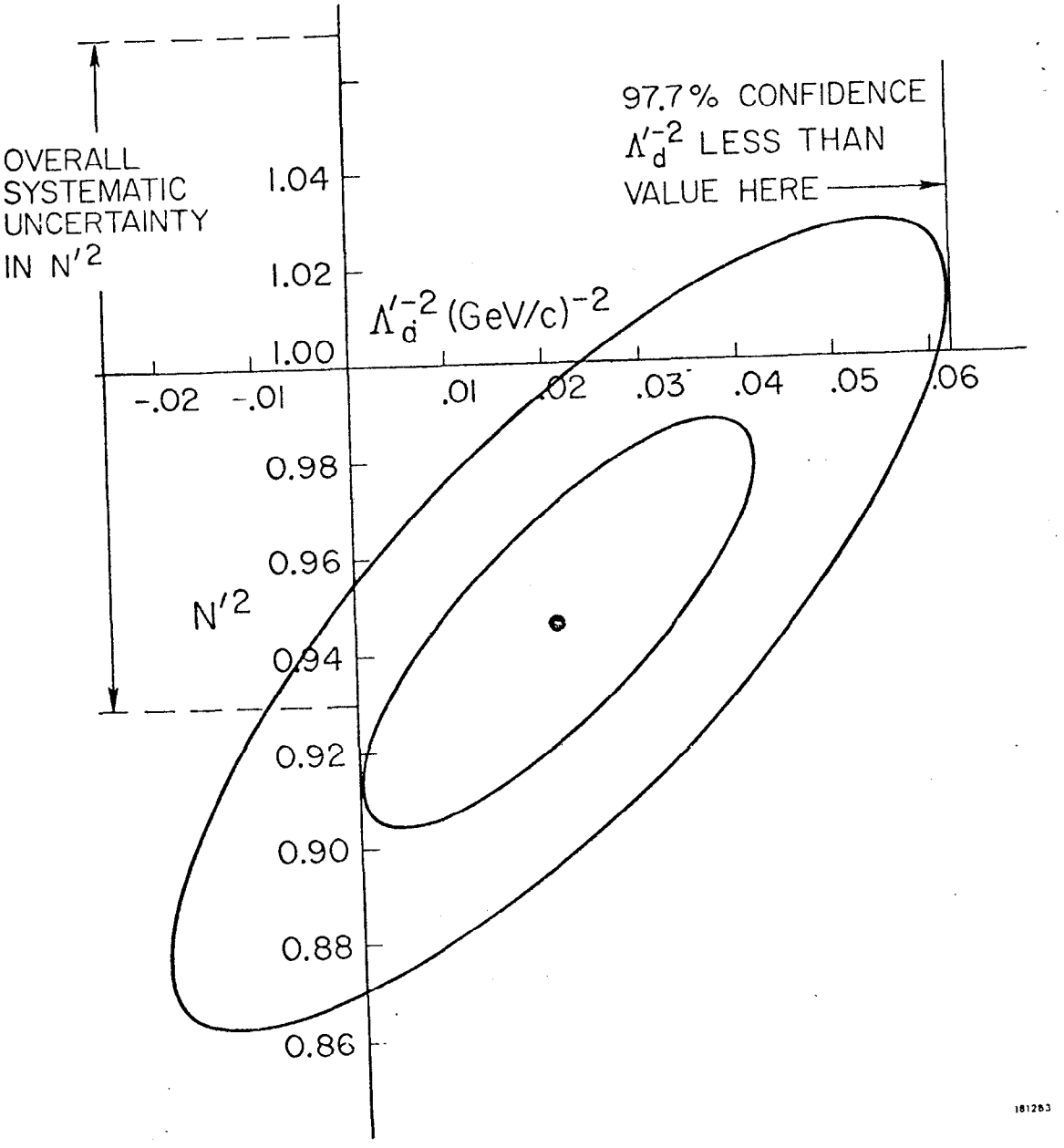
OVERALL
SYSTEMATIC
UNCERTAINTY
IN N'2
97.7% CONFIDENCE
Λ'd-2 LESS THAN
VALUE HERE
1.04
1.02
1.00
Λ'd-2 (GeV/c)-2
-.02
-.01
.01
.02
.03
.04
.05
.06
0.98
0.96
N'2
0.94
0.92
0.90
0.88
0.86
181283

Fig. 18

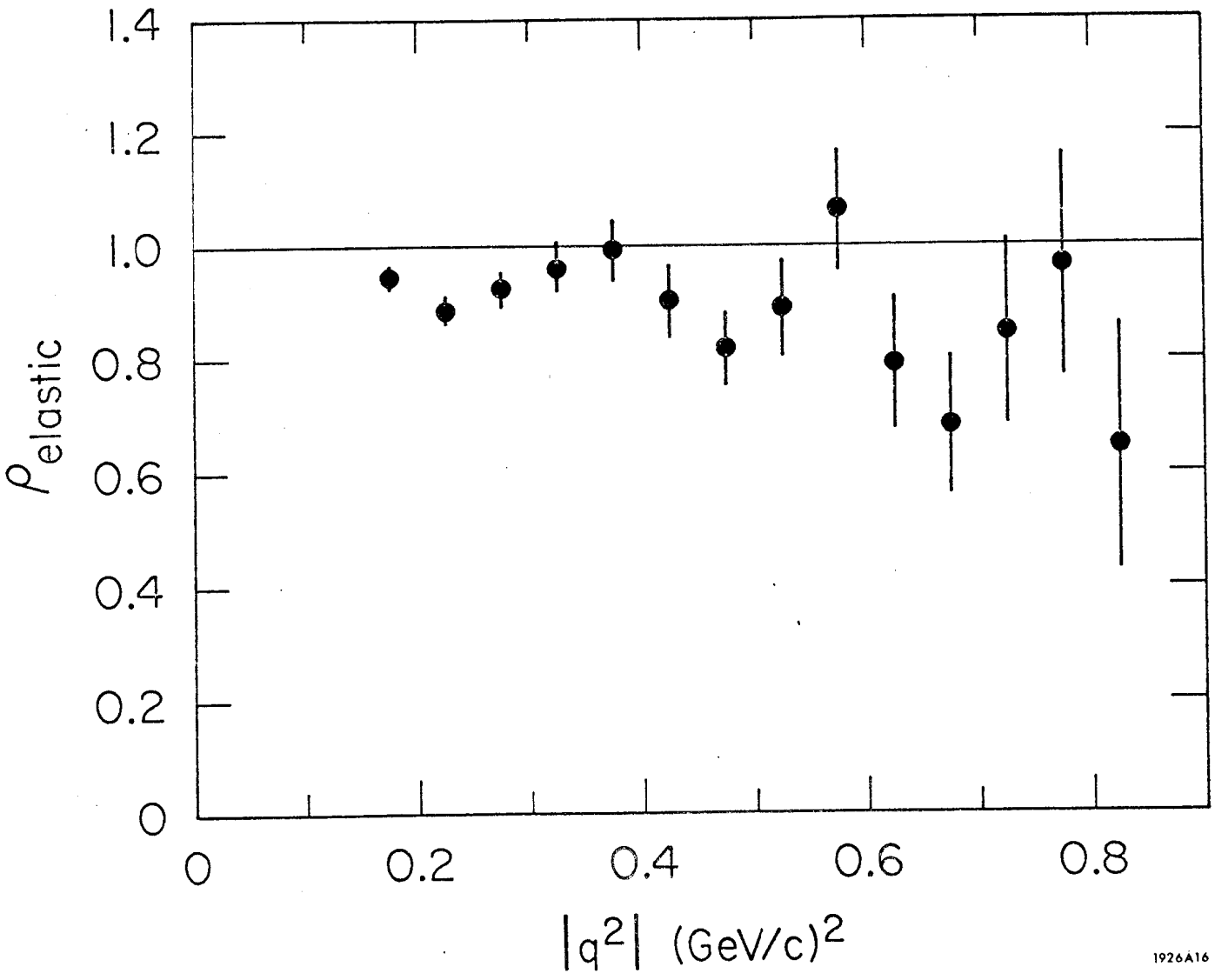

Fig. 19

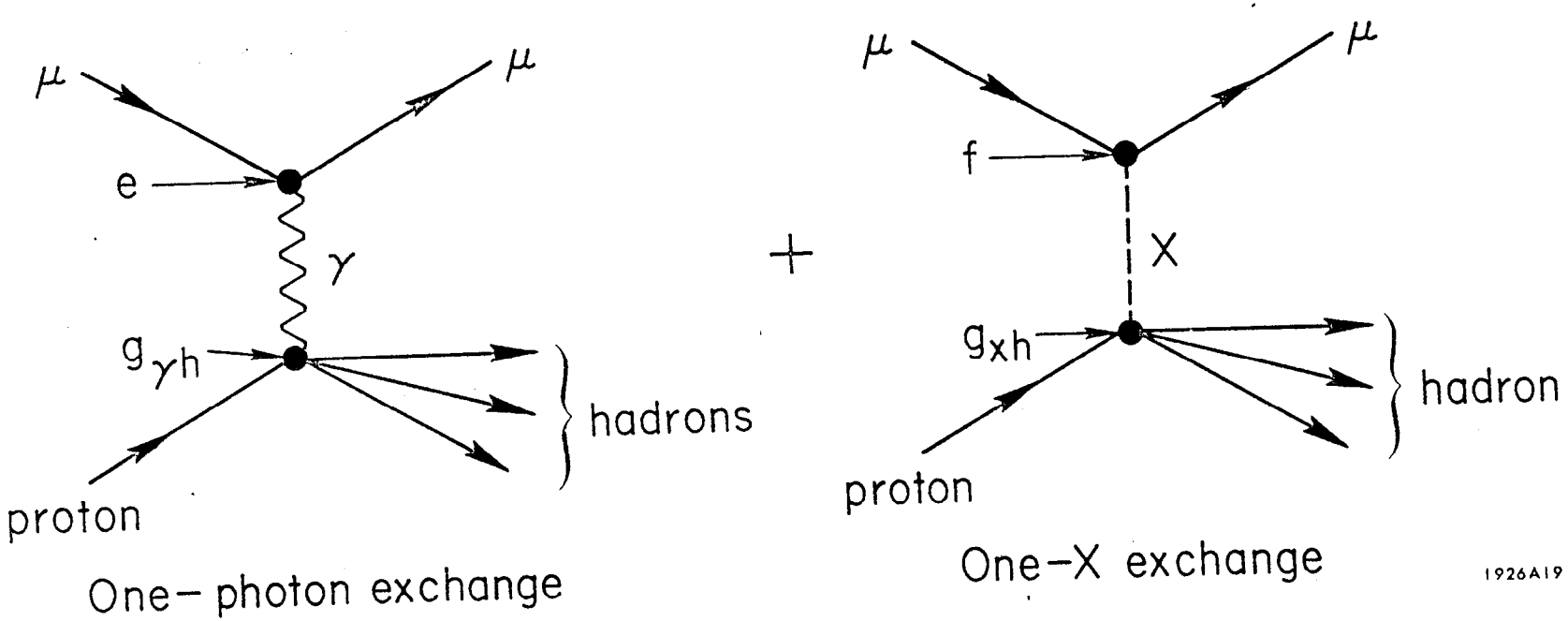
μ
μ
e
γ
$g_{\gamma h}$
hadrons
proton
One- photon exchange
+
μ
μ
f
X
g_{xh}
hadron
proton
One-X exchange
1926A19

Fig. 20